A Plasma Membrane Nanodomain Ensures Signal Specificity during Osmotic Signaling in Plants

Marija Smokvarska, Charbel Francis, Matthieu Pierre Platre, Jean-Bernard Fiche, Carine Alcon, Xavier Dumont, Philippe Nacry, Vincent Bayle, Marcelo Nollmann, Christophe Maurel, et al.

A plasma membrane nanodomain ensures signal specificity during osmotic signaling in plants

Smokvarska M.[1,4], Francis C. [1,4], Platre M.P.[3,4], Fiche J.B. [2], Alcon C.[1], Dumont X.[1], Nacry P.[1], Bayle V.[3], Nollmann M. [2], Maurel C. [1], Jaillais Y.[3], Martiniere A. [1,5,*]

1 BPMP, Univ Montpellier, CNRS, INRAE, Institut Agro, Montpellier, France

2 Centre de Biochimie Structurale, Centre National de la Recherche Scientifique Unité Mixte de Recherche 5048, Institut National de la Santé et de la Recherche Médicale U1054, Université de Montpellier, 34090 Montpellier, France.

3 Laboratoire Reproduction et Développement des Plantes, Université Lyon, École Normale Supérieure de Lyon, Université Claude Bernard Lyon 1, Centre National de la Recherche Scientifique, Institut National de Recherche pour l'Agriculture, l'Alimentation et l'Environnement, F-69342 Lyon, France.

4 these authors contributed equally

5 Lead Contact

* Correpondence: alexandre.martiniere@cnrs.fr

SUMMARY

In the course of their growth and development plants have to constantly perceive and react to their environment. This is achieved in cells, by the coordination of complex combinatorial signaling networks. However, how signal integration and specificity are achieved in this context is unknown. With a focus on the hyperosmotic stimulus, we use live super-resolution light imaging methods to demonstrate that a Rho GTPase, Rho-of-Plant 6 (ROP6), forms stimuli-dependent nanodomains within the plasma membrane (PM). These nanodomains are necessary and sufficient to transduce production of reactive oxygen species (ROS), that act as secondary messengers and trigger several plant adaptive responses to osmotic constraints. Furthermore, osmotic signal triggers interaction between ROP6 and two NADPH oxidases that subsequently generate ROS. ROP6 nanoclustering is also needed for cell surface auxin signaling, but short-time auxin treatment does not induce ROS accumulation. We show that auxin-induced ROP6 nanodomains, unlike osmotically-driven ROP6 clusters, do not recruit the NADPH oxidase, RBOHD. Together, our results suggest that Rho GTPase nano-partitioning at the PM ensures signal specificity downstream of independent stimuli.

INTRODUCTION

Biological membranes can be seen as a patchwork where lipids and proteins are grouped in a juxtaposition of domains of various shapes and sizes. Paradoxically, membranes are also a fluid-structure allowing lateral diffusion of its constituents by thermal agitation. This property of membranes is central as it participates in the dynamic partitioning of proteins and lipids between different plasma membrane (PM) domains and consequently regulates cell-surface signaling processes [1,2]. In plants, the vast majority of PM proteins observed with improved fluorescent microscopy technics was described to be organized in nanodomains of long dwell time (several minutes). It is especially the case of REMORIN3.1 (REM3.1), PLASMA MEMBRANE INTRINSIC PROTEIN2;1 (PIP2;1), PIN-FORMED2 (PIN2), AMMONIUM TRANSPORTER3.1 (AMT3.1), BRASSINOSTEROID INSENSITIVE1 (BRI1), RESPIRATORY BURST OXIDASE HOMOLOG PROTEIN D (RBOHD), FLAGELLIN SENSING2 (FLS2) and NITRATE TRANSPORTER1.1 (NRT1) [3–9]. Nevertheless, the functional relevance of this particular membrane organization remains poorly understood and its role in cell signaling just begins to be explored.

Among other signals, plant cells respond to changes in water availability generated by osmotic constraints. Despite tremendous effort in the last decades, the molecular mechanisms that allow plant cells to perceive and induce early signaling events in response to osmotic stress has just begun to be understood [10,11]. One of the first cellular responses is an accumulation of reactive oxygen species (ROS) [12] in cells, which act as secondary messengers, regulating cell endocytosis but also root water conductivity and intracellular accumulation of osmotica (e.g. proline) [13,14]. Two processes are under action to generate ROS during osmotic signalling. One is non-enzymatic and requires reduction of apoplastic iron. The second is mediated by the PM-localized NADPH oxidases, RBOHD and F [12]. RBOHs catalyze the production of superoxide free radicals by transferring one electron to oxygen from the cytoplasmic NADPH. Even if the mechanism that drives ROS production is now better understood, it is still unclear how it is triggered by a change in osmolarity.

The Rho of plant (ROP), belonging to the super clade of Ras/Rho GTPases, have a key role in cell surface signaling including response to hormones such as auxin or ABA, but also during biotic stimulation [15]. In some cases, they also appear to regulate ROS accumulation, like in tip growing cells or in response to chitin elicitation [16,17]. ROPs are functioning as molecular switches due to a change in conformation between an active GTP-bound form and an inactive GDP-bound form. However, ROP function is also tightly associated with its lipid environment. For instance, the rice type-II ROP OsRAC1 interacts with OsRBOHB in the presence of specific sphingolipids containing 2-hydroxy fatty acids [18]. Besides, the role of charged lipids was recently exemplified in a work on a type-I ROP from *Arabidopsis thaliana*. In this study, the anionic lipid phosphatidylserine (PS) was shown to interact directly with ROP6 C-terminal hypervariable domain, to determine ROP6 organization at the PM and to quantitatively control plant response to the phytohormone auxin [19]. Therefore, the *ROP* gene family may provide good candidates to regulate osmotic signaling.

Here, we show that ROP6 is a master regulator of osmotically-induced ROS accumulation and participates in a set of plant responses to this signal. Using super-resolution microscopy, we found that ROP6 co-exists in the same cell in different states and that osmotic stimulation induces ROP6 nanodomain formation. These nanodomains are needed for a correct ROS accumulation in cells and their composition differs when triggered by other stimuli, suggesting that ROP6 nanodomains may encode for signal specificity.

RESULTS

ROP6 is necessary for osmotically induced ROS accumulation and participates in plant responses to osmotic signal

To investigate the potential role of ROPs in osmotic signaling, we used medium or high sorbitol concentration (ψ_{medium}= -0.26 MPa and ψ_{high}= -0.75 MPa, respectively), and challenged *rop* loss-of-function mutant lines corresponding to the three isoforms that are highly expressed in roots (Figure S1 A). ROS accumulation in cells, as revealed by DHE dye, was used as a fast readout for activation of osmotic signalling (Figure 1B) [12]. Compared to WT, *rop6.2* seedlings, but not *rop2.1* nor *rop4.1*, show impaired ROS accumulation (Figure 1A-C, Figure S1 B). No additive effect was detected in *rop2.1xrop6.2* or *rop2.1xrop6.2*xROP4RNAi (Figure S1 B). The defect in ROS accumulation observed in *rop6.2* is independent of the type of osmoticum (Figure S1 C) and was fully complemented by a transgene containing mCitrine-tagged *ROP6* genomic DNA driven by its promoter (*rop6.*2xmCit-ROP6, Figure 1C). The regulation of ROS signalling was extensively studied in response to PAMPs and ABA. As roots also react to stimulation with Flg22 and ABA, we tested if some of the well-described ROS regulators are involved in osmotically induced ROS (Figure S1 D and E). Whereas the OST1/SNRK2.6 is probably not involved in osmotically-induced ROS production, we found that knock-out plants for *BIK1, BIK1/PLB1* and *CPK5/6/11* show no or attenuated ROS response, respectively. This suggests a potential interaction between osmotic and PAMP signalling, as it was previously postulated [20].

Because ROS accumulation in roots has been tightly associated with deposition of the secondary wall, especially lignin [21], we wondered if an osmotic constraint could enhance cell lignification. Roots exposed to -0.75 MPa for 24 hours have a strong autofluorescence signal compared to control situation, and when stained with phloroglucinol that reveals lignin specifically, a typical cherry-red staining was observed [22] (Figure S2 A and B). We tested if the osmotically-enhanced lignin deposition is indeed associated with ROS accumulation. Loss-of-function plants for the two highly expressed NADPH oxidases (*RBOHD* and *F)*, showed a reduced autofluorescence after exposure to -0.75 MPa and control plants exposed to 1mM H_20_2 for an hour revealed a strong fluorescent signal, showing a connection between osmotically-induced lignin deposition and ROS production (Figure S2 C). This response was partially regulated by ROP6, as *rop6-2* plants show dimmer root autofluorescense signal after -0.75 MPa treatments than control plants either Col0 or *rop6.2*xmCit-ROP6 (Figure S2 C-D).

Interestingly, after 48 hours on -0.75 MPa plate, root tip cells displayed local isotropic cellular growth (Figure S2E). This change in cell polarity has been suggested to reflect an acclimation process of the root facing hyperosmotic condition, as was described for salt or drought responses [23,24]. Because, ROPs are known to regulate cell polar growth of pavement cells, pollen tube and root hairs [15], we wondered if *ROP6* may participate in the osmotically induced cell isotropic growth. *rop6.2* shows a significantly smaller circularity index than wild type or complemented lines on treated plate (-0.75 MPa), whereas no difference between genotypes was found in control conditions (Figure S2 F and G).

Because, ROP6 seems to participate in multiple phenotypes associated to plant acclimation to osmotic constraint, we wondered if *ROP6* can also participate in the changes of root growth and development. Whereas indistinguishable when 5DAG plants were transplanted in control conditions, *rop6.2* plants grew slightly faster than *rop6.2*xmCit-ROP6 in -0.75 MPa plate (rate constant$^{rop6.2\text{xmCit-ROP6}}$ =0.011±0.0005.h^{-1}, rate constant$^{rop6.2}$=0.009 ±0.0008.h^{-1}, t-test p-value=0.02, Figure S2H-K). Indeed, plants have longer primary and lateral roots in loss-of-function *rop6.2* mutant in this stress condition, while no significant effect was observed for lateral root density (Figure S2 L-N). Interestingly, *ROP6* expression pattern fits a potential role in root growth, as

mCit-ROP6 fluorescence is mostly present in the root meristem and elongation zone and in lateral root primordia (Figure S2 O and P). As a whole, ROP6 appears to be necessary for osmotically-induced ROS accumulation, but to some extent it also participates in plant adaptations to hyperosmotic treatments (Figure S2 D, G and K).

ROP6 activation, but not protein quantity, is rate-limiting to trigger osmotic signaling.

Next, we tested if *ROP6* is sufficient to trigger osmotic signaling. Although GFP-ROP6ox overexpressing lines accumulate high amounts of ROP6 proteins, no enhancement of osmotically-induced ROS was observed in control condition or after osmotic treatment, suggesting that ROP activation rather than protein quantity might be a limiting factor (Figure S3 A and Figure 1 C). To test this hypothesis, we used point mutated proteins that are either constitutive active GTP-lock (ROP6-CA) or constitutive inactive GDP-lock (ROP6-DN) ROP6. Transient expression in tobacco leaves of FRET based sensors (iROP) shows that ROP6-CA but not ROP6-DN interacts with the CIRB domain of PAK1, confirming their respective GTP or GDP-lock behavior (Figure S3 B, C and D). Stable *rop6.2* plants expressing mCit-ROP6-CA, under its endogenous promotor, showed a constitutively high ROS accumulation, independent of the stimulus (Figure 1 D). Oppositely, in *rop6.2x*mCit-ROP6-DN plants, ROS induction was attenuated after exposure to -0.75 MPa and totally suppressed after -0.26 MPa treatments, compared to a control situation (Figure 1 D). This suggest that ROP6 itself might be sufficient for a part of the osmotically-induced ROS production.

These results showed that ROP6 is necessary and its activation sufficient to trigger ROS production. Then, we addressed if ROP6 activation could act upstream of ROS producing enzymes. Therefore, rop6.2xmCit-ROP6-CA line, that has constitutively high ROS, was treated alone or in combination with specific inhibitors for each of the two ROS pathways activated by the osmotic stimulus [12]. Diphenyleneiodonium (DPI) was used to inhibit NADPH oxidase activity and bathophenanthrolinedisulfonic acid (BPDS) to block ROS mediated by ferric iron[12]. In co-treatment, ROS generated by mCit-ROP6-CA is diminished drastically, suggesting that mCit-ROP6-CA is acting upstream of ROS production machinery (Figure 1 E). Next, we determined if ROP6 activation is associated with a change in its subcellular localization, as described for many small GTPases [25]. A sharp fluorescent signal was observed delimiting root cells expressing mCit-ROP6, which overlaid with the FM4-64 PM dye (Figure S2 Q). Only a minor difference in PM fluorescence intensity or relative PM localisation was observed between wild type and GTP or GDP lock ROP6 (Figure S3 E, F and G), suggesting that ROP6 is at most marginally regulated by cytoplasmic/PM shuttling.

Two populations of ROP6 molecules co-exist within the plasma membrane and vary in frequency minutes after osmotic treatment

We recently showed that ROP6 organization at the PM is critical for auxin signalling[19]. We thus addressed whether ROP6 lateral segregation at the PM could contribute to osmotic signaling. Total internal reflexion fluorescent microscopy (TIRFM) in two independent transgenic lines showed that GFP-ROP6 has a uniform localization within the PM in control conditions, while in -0.26 MPa and even more in -0.75 MPa treated cells, GFP-ROP6 appeared in diffraction-limited spots at the cell surface (Figure 2 A and B). This suggests that ROP6 clustered in response to osmoticum treatment in a dose-dependent manner (Figure 2 B). Kymograph analysis showed straight lines for up to 50 seconds, suggesting that GFP-ROP6 clusters are stable within the PM during this period (Figure 2 C). We then wondered if ROP6 clustering could not go along with its dissociation from the PM. Indeed, GFP-ROP6 shows a lower PM association index after osmotic treatment (Figure S3 H and I). When ROP6 was locked in GTP bound form (RFP-ROP6-CA), this effect was not observed although this form was able to cluster (Figure S3

H, I, J and K). Taken together, this suggests that ROP6 clustering and its membrane dissociation are not strictly linked.

The average GFP-ROP6 spot size is close to the limit of diffraction (radius = 235 +/- 60.57 nm). Therefore, we next used sptPALM, a super-resolution imaging technic, recently developed on plant samples [12,19,26]. Upon stochastic photoswitching on live roots expressing mEOS2-ROP6, sub-diffraction spots are appearing with blinking behaviour and small life span (< 0.5sec), as expected from single molecule behaviour (Video S1 and Figure S4 A and B). By retrieving the displacement of each ROP6 single molecule along with the videos, two behaviours can be observed in control condition (Figure 2 D, highly diffusible molecules in orange and lowly diffusible molecules in blue, Figure 2 E). Distribution of instantaneous diffusion coefficient of ROP6 single molecules, extrapolated from mean square displacement plots, is bimodal (Figure 2 F, green curve Figure 2 G). This result shows that diffusible (D_{diff}=0.05+/-0.007µm².s^{-1}) and relatively immobile (D_{imm}=0.002+/-0.0007µm².s^{-1}) mEOS2-ROP6 molecules coexist within the PM of a single cell. Minutes after -0.75 MPa treatments, the frequency of immobile mEOS2-ROP6 doubles (Figure 2 G, H and I). Clustering analysis on live PALM images, using Vonoroï tessellation [27] (Figure 2 J), showed that the occurrence of molecules with high local density increases after -0.75 MPa treatment (Figure 2 K and L, $Log_{local\ density}$>3). Nevertheless, at this stage it was not possible to distinguish between three different cases: (i) the sizes of nanodomains are increasing after treatment, (ii) cells have the same number of nanodomains between control and treatment but with more ROP6 molecules in it or (iii) more nanodomains are formed in response to -0.75 MPa, with a similar amount of ROP6 protein. To distinguish between these possibilities, segmented images were generated based on detection local density, where only ROP6 molecules with a local density higher than $Log_{local\ density}$>3 were investigated (Figure S3 C, D and E). Whereas no effect on domain size, nor percentage of mEOS-ROP6 molecules per nanodomains was found, the density of nanodomains per µm² of PM doubles after osmotic treatment (Figure 2 M-O). Together our results suggest that in response to osmotic stimulation, ROP6 molecules are clustering in nanometer-sized domains (i.e. nanodomains), with a relatively fixed size and constant number of ROP6 molecules, and in which ROP6 barely diffuses. This ROP6 diffusion behaviour differs substantially from what we know for other PM proteins, such as the P-type ATPase, AHA2, or the aquaporin, PIP1;2, which show an enhanced diffusion when cells are exposed to hyperosmotic stimulation [12].

ROP6 nanodomains are necessary to trigger osmotically-induced ROS

Next, we addressed whether ROP6-containing nanodomains are involved in osmotic signaling. Because GTP-locked ROP6 (ROP6-CA) is constitutively producing ROS (Figure 1 D), we quantified diffusion and local density of mEOS2-ROP6-CA molecules by sptPALM. In comparison to the wild-type protein, ROP6-CA has a higher proportion of immobile molecules and a bigger fraction of molecules with high local density in control condition. No difference was recorded between ROP6 and ROP6-CA after treatment, suggesting that ROP6-CA is constitutively associated with nanodomains (Figure 3 A, B and C). In addition to its C-terminal prenylation, ROP6 is transitorily S-acylated on cysteines 21 and 158 [17]. These modifications are required for localization in detergent-resistant membranes and cause retarded lateral diffusion of the constitutive active GTP-lock ROP6 but have no impact on ROP6 GTPase activity or PM targeting [17]. To test if ROP6 acylation is required for nanoclustering, we generated mEOS2-ROP6$^{C21S/C158S}$ expressing plants. Using sptPALM and clustering analysis, we found that mEOS2-ROP6$^{C21S/C158S}$ was insensitive to -0.75 MPa treatments (Figure 3 D, E and F). Because mEOS2-ROP6$^{C21S/C158S}$ is not associated with nanodomains in response to osmotic treatment, we compared the ROS response in *rop6.2*xmCit-ROP6$^{C21S/C158S}$ and *rop6.2*xmCit-ROP6 complemented lines. Treatments with -0.26 MPa or -0.75 MPa did not trigger any ROS accumulation in *rop6.2*xmCit-ROP6$^{C21S/C158S}$ (Figure 3 G). Importantly, mCit-ROP6$^{C21S/C158S}$ expressed under the control of its own promoter localized at the PM in root cells (Figure 3 H and I),

as previously reported for 35S::GFP-ROP6-CA$^{C21S/C158S}$ in leaves [17]. Together, our results suggest that ROP6 nanodomain formation, rather than only ROP6 PM localization, is necessary to activate osmotic signaling in cells.

Activated ROP6 interacts with RBOHD and F in PM nanodomains to generate ROS

We checked first if *ROP6*, *RBOHD* and *RBOHF* are co-expressed in similar Arabidopsis root cells. Transcriptional fusion for RBOHD, and translational fusion for ROP6 and RBOHF all showed an expression signal in root epidermis (Figure S5 A, B and C). Next, we tested if the two NADPH oxidases isoforms that are activated by osmotic signal, RBOHD and RBOHF, could interact with ROP6. FLIM experiments were performed in tobacco leaf cells that transiently expressed the two putative interacting proteins tagged with GFP or mRFP. We found a significant diminution of GFP life time when GFP-RBOHD was co-expressed with RFP-ROP6-CA compared to cells expressing GFP-RBOHD and RFP-ROP6-DN or when cells expressed only the donor GFP-RBOHD (Figure 4 A and B). Similar results were observed with GFP-RBOHF, suggesting that both RBOHs interact *in planta* with the GTP-, but not the GDP-locked form of ROP6 (Figure S5 D). This is in line with recent observations made in yeast two hybrid experiments, where RBOHD and ROP6-CA were shown to interact [28].

Because ROP6 and RBOHs physically interact and ROP6 forms nanodomains that are necessary for ROS accumulation, we hypothesized that RBOHs could also be organized in nanodomains in the cell PM. Arabidopsis lines overexpressing GFP-tagged RBOHD and RBOHF were generated. Under TIRF illumination, GFP-RBOHD showed a uniform localization in control condition, while 2 minutes after -0.75 MPa treatment, cells had clearly visible spots (Figure 4 C and D). By using GFP-RBOHDxRFP-ROP6 plants, we observed that ROP6 accumulated in the same structure as RBOHD after osmotic stimulation (Figure 4 E and F). As *rbohF* and *rbohD* mutant plants display similarly reduced ROS accumulation in response to osmotic stimulation, we tested if RBOHF would form stimuli-dependent clusters in the PM, like RBOHD does [12]. Eventhough there was a substantial number of detectable clusters in control condition, GFP-RBOHF overexpressing plants showed an increased cluster density minutes after -0.75 MPa treatment, though less than in the case of RBOHD (Figure S5 E and F). This last result suggests that to some extent both RBOHD and RBOHF have a re-localisation behaviour in response to osmotic stimulation. Then, to analyse whether RBOH domains formation is a consequence of ROP6 activation or is triggered through an independent pathway, we crossed Col0 GFP-RBOHD line with RFP-ROP6-CA or *rop6.2*. The density of GFP-RBOHD clusters is much higher when the constitutively active form of ROP6 is present in cells, even in the absence of any stimulation (Figure 4G and H). In the case of ROP6 loss of function plants, GFP-RBOHD is observed in clusters in control condition, and its density did not change after cell stimulation (Figure 4 G and I). Since GFP-RBOHD clusters are present in the absence of ROP6, and since an active ROP6 is likely required for RBOH function in response to osmoticum, these last results suggest that GFP-RBOH cluster formation is not strictly associated to ROS production.

To confirm that RBOHD/ROP6 nanodomains are acting as a functional unit for ROS production in the plant cell, we tested whether ROP6 nanodomain formation is caused and is not a consequence of ROS production. Neither inhibition of ROS by DPI/BPDS nor H2O2 treatment have any impact on ROP6 nanodomain formation (Figure S5 G, H and I). Most importantly, we also tested if an osmotic signal can trigger the interaction between ROP6 and RBOHD in Arabidposis roots. FLIM experiment was performed in Arabidposis roots expressing GFP-RBOHD and wild type or constitutive active ROP6. A significant decrease of life time was observed 5 minutes after osmotic treatment with the GFP-RBOHDxRFP-ROP6 plant, but not when GFP-RBOHD is alone nor with GFP-RBOHDxRFP-ROP6-CA which display constitutive low FLIM as expected (Figure 4 J and K). Thus, a

RBOHD/ROP6 complex is formed in membrane nanodomains upon cell stimulation. This structure is necessary but not sufficient for osmotically-induced accumulation of ROS in cells.

Can ROP6 nanodomain formation mediate independent signaling events?

ROP6 is necessary for several plant signaling responses including to the phytohormone auxin [14,18,27]. The correct targeting of the auxin transport efflux carrier PIN2 is mediated by ROP6 and therefore participates in root gravitropic response [27,18]. Recently, ROP6 nanodomain formation, mediated by the anionic lipid phosphatidylserine (PS), was described in response to auxin [19]. Together with our results on osmotic signaling, this suggests that nanodomain formation is a general feature of ROP6 signaling pathways in plants (Figure 5 A and B). We addressed whether RBOHD clustering is also induced in response to auxin stimulation, as it happens after the induction of osmotic signaling pathway. No increase of GFP-RBOHD clusters density was observed in such condition, whereas ROP6 clearly show, as expected, numerous dotted structure in the PM (Figure 5 A and B). As it was previously described, roots exposed to auxin for a short time (60 min) failed to accumulate ROS, which contrasts with osmotic stimulation (Figure 5 C) [31–34]. These results show that ROP6 nanoclusters formed after auxin or osmotic stimulations can differ in their constituent and consequently encode, to a certain extent, for signal specificity.

DISCUSSION

By combining genetic and super resolution live imaging, we showed that ROP6 forms osmotic specific nanodomains within the PM that are required to trigger secondary messenger in cells. The role of this specific ROP isoform is central for osmotic signaling since *rop6.2* has a totally abolished osmotically-induced ROS production. In contrast, ROP2 and ROP4 which are also highly expressed in roots are dispensable for osmotic signalling [34]. In addition, we found that ROP6 controls some terminal plant responses to osmotic stress. Indeed, loss of function plants for *ROP6* exhibit less osmotically-induced lignin deposition in their roots. Lignin polymerisation requires cellular ROS. This was for example demonstrated in the case of Casparian strip formation, where the NADPH oxidase, RBOHF, is localised in specific membrane domains to produce ROS that permit a spatialy targetted polymerisation of monolignol [21,35]. It is therefore likely that osmotically-induced lignin deposition is also mediated by ROS but from ROP6/RBOHs nanodomains. This enhancement of lignin synthesis in response to hyperosmotic stimulation could participate in plant acclimation to stress conditions. Indeed, lignin increases cell wall stiffness and may protect cells from deformation due to turgor loss. Secondary walls are also known to counteract mineral and water leakage in roots [36,37]. Enhanced lignin deposition may participate in such phenonena during long term osmotic treatment. In addition, we observed that cells under elongation form spheres rather than cylinders when exposed to a hyperosmotic treatment. This tendency to isotropic cell expansion could minimize tension and consequently could prevent cell bursting. ROPs are known regulators of cell polarity in pavement cells or tip growing cells. In particular, it was demonstrated that they can participate in cytoskeleton remodelling throught interaction with RIC1 and katanin [38]. Here, the need for ROP6 to ensure cell isotropic expansion and modified root elongation in response to stress condition not necessarily involves ROS production but could be mediated by other types of effector proteins. Thus, we believe that ROP6 is an important factor for plant osmotic signaling, likely acting right after cell osmotic perception, as ROP6 nanodomain formation happens only minutes after cell stimulation. Its role in long term adaptation is likely more indirect.

We also demonstrated that, upon cell activation by osmotic stimulation, enhanced ROS accumulation is associated with the formation of a ROP6/RBOHD complex within the PM. Plants expressing a GTP-lock form of ROP6 show a higher cellular accumulation of ROS. In this genetic background, ROP6 nanoclustering and its colocalization with RBOHD happen without any cell stimulation. These results fit with our FLIM experiment, where RBOH interacts preferentially with ROP6 GTP-locked form. On the other hand, *rop6* plants complemented with mutated ROP6 that are unable to be acylated, loose both the osmotically-induced nanodomain formation and consequently the ROS accumulation after hyperosmotic stimulation. But how can ROP6/RBOH complex get into nanodomains? The constitutive active ROP6 (ROP6-CA) was shown to be associated with detergent resistant membranes together with a slower diffusion [17,19]. This behaviour is mediated firstly by acylation of C23 and C158 residues of the protein with palmitic and/or stearic acids and secondly by the direct binding between lysine residues in ROP6 hypervariable tail and phosphatidylserine (PS) [17,19]. These results suggest, like for their animal and yeast counterpart, plant small GTPases have a greater affinity for specific lipid environment when they are activated, which then determine their nanoclustering [39–41]. Because activated ROP6 is interacting with RBOHs, we think that the former might drag and/or retain RBOHs protein to ROP6 nanodomains. This is supported by the fact that ROP6-CA can alone induce RBOH clustering and that in ROP6 loss-of-function mutants, GFP-RBOHD clustering is not inducible by osmotic stimuli. Nevertheless, we also observed that the basal level of RBOH clusters in r*op6.2* is higher than in control plant. Thus, RBOH can make clusters in the absence of ROP6. In this case, however, the clusters are not associated with ROS production and suggesting that ROP6 could act as a negative regulator.

Our group has recently described that two ROS machineries are under action in response to osmotic stimulation, one of these involving two isoforms of NADPH oxidase, RBOHD and F [12]. Our results suggest that ROP6 is an upstream regulator of both ROS generating pathways (Figure1 C and E). However, we also found that ROP6-DN expressed at its native level is able to partialy rescue the ROS-release phentotype of *rop6.2* under high stress conditions. Since ROP6-DN cannot interact with PAK1 nor RBOHD and F, we believe that ROP6-DN may act as a scaffold for the ROS producing machinery that is independent of RBOH. On the other hand, the role of ROP6 on RBOH-dependant ROS production is rather associated with nanodomain formation. However, how recruitment of RBOHs in ROP6 nanodomains can regulate ROS accumulation is still unclear. Because of it ability to generate potentially harmful oxygen radicals, RBOH activity is tightly controlled in cells. This is particularly well described for pathogen elicitors, whereby several protein kinases including BIK1 and CPK5 are necessary for PTI mediated ROS accumulation and can directly phosphorylate RBOHD N-terminus [42,43]. The change in RBOH PM localization, as mediated by ROP6, could participate in RBOH interaction with protein kinases and consequently alter RBOH phosphorylation/dephosphorylation kinetic. Also, RBOHD and F contain EF-hands that can directly bind calcium and are essential for RBOH activity [44,45]. Within the cell membrane, calcium gradients might exist in the vicinity of calcium membrane transporters [46]. Therefore, recruitment of RBOH proteins in ROP6-containing nanodomains that would also harbour these calcium transporters could alter RBOH micro-environment, thereby regulating its activity. In addition, RBOH dimerization was observed from purified OsRBOHB N-terminus but was also suggested from step bleaching experiment done *in vivo* [7,47]. Interestingly, we observed an epistatic interaction between *rbohD* and *rbohF* for osmotically induced ROS, suggesting that RBOHD and F might form heteromers [12]. Similar observations were recently described for ROS triggered upon cell ablation [48]. We speculate that co-clustering of RBOHD and RBOHF in ROP6-containing nanodomains could increase their probability to form functional heteromers.

Rho GTPases are generally seen as the neck of an hourglass for signal integration at the cell surface. Indeed, multiple input pathways converge on a single Rho GTPase, leading to various downstream cellular outputs, which are often specific to the upstream signal. How signaling specificity is achieved in this context is an outstanding unresolved question. In our work, we found that a single ROP isoform could, in response to different stimuli e.g. auxin and osmotic stimulus, generate very similar nanodomains in terms of shape, cellular density or even size [19]. Nevertheless, we also found that these nanoclusters differ in their composition, in at least RBOH proteins. Therefore, the segregation of signaling components in distinct plasma membrane nanodomains can generate signal specificity downstream of a single small GTPase. How this discrimination happens still remains an open question. It could be because of specific lipid environment or/and recruitment of additional proteins that will participate in the stabilization of ROP6/RBOH complexes.

ACKNOWLEDGMENTS

We thank the Montpellier Ressources Imagerie (MRI) and the Histocytology and Plant Cell Imaging Platform for providing the microscope facility (PHIV). Y.J. was funded by ERC no. 3363360-APPL under FP/2007-2013; Y Y.J. and A.M. by the innovative project iRhobot from the department of "Biologie et Amélioration des Plantes" (BAP) of INRAE, A.M. is founded by the French National Agency ANR CellOsmo (ANR-19-CE20-0008-01)

AUTHOR CONTRIBUTIONS

M.S. and A.M. conceived the study; M.S., C.F., M.P.P., C.A., X.D., N.P. and V.B. performed experiments; M.S., A.M., J.B.F. and P.N. analyzed data; J.B.F. and M.N. designed the TIRF microscopes and the sptPALM analysis pipline. C.A. gave advice about the FLIM imaging procedure; C.M., Y.J. and A.M. prepared figures and wrote the manu-

script with input from all co-authors; and all authors read and approved the final version of the manuscript

DECLARATION OF INTERESTS

The authors declare no competing interests

FIGURE LEGENDS

Figure 1: ROP6 activation is necessary and sufficient to trigger osmotically driven ROS accumulation in Arabidopsis root cells. (A) Drawing of Arabidopsis plantlets, where the red square highlights the part of root under study. (B) Dihydroethidium (DHE) stained root cell of Col0, *rop6.2* and *rop6.2*xmCit-ROP6 in control condition (0 MPa) or after 15 min of -0.75 MPa treatment. (C-D) DHE fluorescence quantification after 15 min treatment with 0, -0.26 or -0.75 MPa solution in different genetic materials: Col(0), *rop6.2*, ROP6 over expresser line (GFP-ROP6ox) and *rop6.2* lines expressing under ROP6 endogenous promotor, either ROP6 (mCit-ROP6 (*rop6.2*xmCit-ROP6), the constitutive active ROP6 (*rop6.2*xmCit-ROP6-CA) or the dominant negative (*rop6.2*xmCit-ROP6-DN). (E) ROS quantification (DHE fluorescence) in root cells expressing the constitutive active ROP6 (mCit-ROP6-CA) in control or after mild or high osmotic stimulus (respectively 0, -0.26 and -0.75 MPa) supplemented or not with ROS enzyme inhibitors. DPI was used for inhibition of NADPH oxidase activity and BPDS to inhibit ROS produced from ferric iron. Error bars correspond to a confidence interval at 95%. ANOVA followed by Tukey test, letters indicate significant differences among means (p-value<0.001). n>49 from 4-6 independent biological replicates. Scale bar 20 µm.

See also Figure S1, S2 and S3.

Figure 2: Osmotic stimulus triggers ROP6 molecular nanoclustering at the PM (A) TIRFM micrograph of oxGFP-ROP6 expressing cells after 2 min incubation with solutions at either 0 MPa, -0.26 or -0.75 MPa. (B) Quantification of ROP6 cluster density. (C) Kymograph image of oxGFP-ROP6 clusters from cells exposed to 0.75 MPa. Clusters at initial time point are labelled with arrows. (D) Image reconstruction of around 5 000 single mEOS2-ROP6 molecule trajectories in two control cells. (E) Close-up view of cell expressing mEOS2-ROP6, where trajectories with high or low diffusion instantaneous coefficient labelled in orange or blue respectively. (F) Mean square displacement curves of the highly or lowly diffusible molecules in control (0 MPa) or treatment (-0.75 MPa) conditions. (G) Bimodal distribution of molecule instantaneous diffusion coefficients in control (0 MPa, green curve) and treatment (-0.75 MPa, purple curve) conditions. (H) Close up view of the PM of cells expressing mEOS2-ROP6 2 minutes after a -0.75 MPa treatment. (I) Histogram represents the percentage of molecules with an instantaneous diffusion below 0.01 $um^2.s^{-1}$ in control (0 MPa) or after treatment (-0.75 MPa). (J) Vonoroï tessellation of mEOS2-ROP6 molecules localization map from the exact same two control cells of (D). Top right inset is a close up view, showing a mEOS2-ROP6 nanodomain. (K) Distribution of molecules local density in control (0 MPa, green curve) and treatment (-0.75 MPa, purple curve) conditions. (L) Percentage of molecules with a log(local density) higher than 3. (M) Distribution of the mEOS2-ROP6 nanodomains diameter in control (0 MPa) and treatment (-0.75 MPa) conditions. (N) Relative occurrence of mEOS2-ROP6 in nanodomains in control (0 MPa) and treatment (-0.75 MPa) conditions. (O) Nanodomain density in control (0 MPa) or after 2 minutes treatment with -0.75 MPa solution. Error bars correspond to a confidence interval at 95%. For (B) an ANOVA followed by Tukey test was done, letters indicate significant differences among means (p-value<0.001). * p-value below 0.01 T-Test. n>12 from 3 independent biological replicates. Scale Bar 10µm, except for E and H where it is 1 µm.

See also Figure S3, S4 and Video S1

Figure 3: ROP6 nanoclustering is required for ROS accumulation. (A) Bimodal distribution of mEOS2-ROP6 instantaneous diffusion (green curve) or mEOS2-ROP6-CA (purple curve) in control condition (0 MPa). (B) Histogram represents the percentage of molecules with an instantaneous diffusion below 0.01 $um^2.s^{-1}$ in mEOS2-ROP6 and mEOS2-ROP6-CA expressing lines in control (green) or after osmotic stimulation (purple). (C) Percentage of molecules with a log(local density) higher than 3 in mEOS2-ROP6 and mEOS2-ROP6-CA expressing lines in control (green) or after osmotic stimulation (purple). (D) Bimodal distribution of mEOS2-ROP6$^{C21S/C158S}$ instantaneous diffusion coefficients in control (0 MPa, green curve) and treatment (-0.75 MPa, purple curve) conditions. (E) Histogram represents the percentage of mEOS2-ROP6$^{C21S/C158S}$ molecules with an instantaneous diffusion below 0.01 $um^2.s^{-1}$ in control (0 MPa) and treatment (-0.75 MPa) conditions. (F) Percentage of mEOS2-ROP6$^{C21S/C158S}$ molecules with a log(local density) higher than 3. (G) Quantification of ROS accumulation by DHE staining in *rop6.2*xmCit-ROP6 or *rop6.2*xmCit-ROP6$^{C21S/C158S}$ expressing cells after 15 min treatment with 0, -0.26 or -0.75 MPa solution. (H) Plasma membrane localization of mCit-ROP6 and mCit-ROP6$^{C21S/C158S}$ and its relative amount at the PM (I). Error bars correspond to a confidence interval at 95%. * p-value below 0.01 *t*-test. ns. Non-significant. n>9 from 3 independent biological replicates. Scale bar 10µm.

Figure 4: ROP6 interacts and forms nanoclusters with RBOHD at the PM. (A) GFP-RBOHD fluorescence lifetime when co-expressed with dominant negative (RFP-ROP6-DN) or constitutive active ROP6 (RFP-ROP6-CA) in transient expression in tobacco leaf epidermal cells and its quantification (B). (C) TIRF micrograph of cell expressing GFP-RBOHD in control or after 2 minute treatment with -0.75 MPa solution and quantification of clusters density (D). (E, F) Cell co-expressing GFP-RBOHD with RFP-ROP6 in control (E) or after -0.75 MPa treatment (F). Graphs below represent the pixel intensity along the dotted line in each of the conditions. (G) TIRFM micrograph of GFP-RBOHD signal in GFP-RBOHDxRFP-ROP6, GFP-RBOHDxRFP-ROP6-CA and *rop6.2*xGFP-RBOHD plant in control or after -0,75 MPa incubation and their respective quantification (H and I). (J) GFP-RBOHD fluorescence lifetime when expressed alone or co-expressed with RFP-ROP6 or RFP-ROP6-CA in root cells and its quantification (K). Error bars correspond to a confidence interval at 95%. For (B) an ANOVA followed by Tukey test was done, letters indicate significant differences among means (p-value<0.001). * p-value below 0.01 T-Test. n>12 from 3 independent biological replicates. Scale bar 10µm.

See also Figure S5

Figure 5: Auxin-stimulated ROP6 nanodomains are free of RBOHD. (A) TIRFM micrograph of cell expressing GFP-ROP6 or GFP-RBOHD in control condition (DMSO) or after 10 µM NAA for 1 hour. (B) Cluster density quantification after NAA or -0,75 MPa treatment. (C) Quantification of ROS accumulation by DHE staining in control (DMSO) or after 15 min treatment with 10 µM NAA. Error bars correspond to a confidence interval at 95%. For (B) an ANOVA followed by Tukey test was done, letters indicate significant differences among means (p-value<0.001). * p-value below 0.01 T-Test. n>11 from 3 independent biological replicates. Scale bar 10µm.

STAR METHODS

Detailed methods are provided in the online version of this paper and include the following

CONTACT FOR REAGENT AND RESOURCE SHARING

Further information and requests for resources and reagents should be directed to and will be fulfilled by the Lead Contact, Alexandre Martiniere (alexandre.martiniere@cnrs.fr)

MATERIEL AVAILABILITY STATEMENT

Arabidposis lines and plasmids generated in this study are availaible upon request to the Lead Contact, Alexandre Martiniere (alexandre.martiniere@cnrs.fr).

DATA AND CODE AVAILABILITY STATEMENT

This study did not generate any code and the published article includes all dataset analyzed during this study.

EXPERIMENTAL MODEL AND SUBJECT DETAILS

Plant material

Arabidopsis thaliana accession Col-0 was used as wild type in this study. The following lines were published before: *rop6.2* [29], *rop2.1* [49], *rop4.1* [50], *rop6.2*x*rop2.1* [51], *rop6.2*x*rop2.1*xROP4RNAi [51], *rop6.2*xpROP6:mCit-ROP6g [19], p35S:mEOS-ROP6g [19], p35S:mEOS-ROP6g-CA [19], pRBOHD:nls-GUS-GFP [19], pRBOHF:mcherry-RBOHFg [21] and *bik1* [52], *bik1*x*pbl1* [53], *cpk5/6/11* [54] and *ost1.2*[55]. Information on all genes referenced in this work, including mutant alleles and sources is provided in Table S1.

METHOD DETAILS

Growing conditions and plant materials:

Plants were stratified for 2 days at 4°C and grown vertically on agar plates containing half-strength Murashige and Skoog (½ MS) medium supplemented with 1% (w/v) sucrose and 2.5mM MES-KOH pH6 for 5 days at 22°C in a 16-h light/8-h dark cycle with 70% relative humidity and a light intensity of 200 $\mu mol \cdot m^{-2} \cdot s^{-1}$, prior to use. *Nicotiana tabacum* used for transient expression were grown in soil at 22°C in a 8-h light/16-h dark cycle with 70% relative humidity and a light intensity of 200$\mu mol \cdot m^{-2} \cdot s^{-1}$. For root architecture analyses, seedlings were grown on vertical square 12x12 cm Petri dishes in a self-contained imaging unit equipped with a 16M pixel linear camera, a telecentric objective and collimated LED backlight. Plants were grown in the imaging automat dedicated growth chamber at 23°C in a 16-h light/8-h dark cycle with 70% relative humidity and a light intensity of 185 $\mu mol \cdot m^{-2} \cdot s^{-1}$ (Vegeled Floodlight, Colasse Seraing – Belgium). Plates were imaged every four hours allowing fine kinetic analysis.

Cloning and plant transformation

The vector ROP6g/pDONRP2RP3, which includes the full ROP6 genomic sequence from ATG to the end of its 3'UTR (ROP6g – At4g35020) [19] was amplified with the overlapping primers to generate either ROP6g-CA/pDONRP2R (G15V) or ROP6g-DN/DONRP2RP3 (T20N). ROP6g-CA/pDONRP2R-P3 and ROP6g-DN/pDONRP2R-P3 were

then recombined by LR multisite reaction with ROP6prom/pDONRP4P1R [19], mCITRINEnoSTOP/pDONR221 [56] and pB7m34GW [57] to generate pROP6:mCit-ROP6g-CA and pROP6:mCit-ROP6g-DN vectors, respectively. ROP6g/pDONRP2RP3 was amplified with overlapping primers to generate ROP6gC21S-C158S/pDONRP2RP3. ROP6gC21S-C158S/pDONRP2R-P3 was then recombined by LR multisite reaction with 2x35Sprom/pDONRP4P1R [58], mEOS2noSTOP/pDONR221[19] and pB7m34GW [57] to generate p35S:mEOS2-ROP6C21S-C158S. ROP6gC21S-C158S/pDONRP2R-P3 was also recombined by LR multisite reaction with ROP6prom/pDONRP4P1R [19], mCITRINEnoSTOP/pDONR221 [56] and pB7m34GW [57] to generate ROP6prom:mCITRINE-ROP6C21S-C158S. The coding sequence of RBOHD (At5g47910), RBOHF (At1g64060), ROP6 (At4g35020), ROP6-CA (G15V) and ROP6-DN (T20N) were PCR amplified and inserted into pENTR/D-TOPO. pB7WGF2 and pB7WGR2vector were used as destination vector for respectively GFP and RFP fusion. The unimolecular FRET sensor with intact C-terminus was designed based on RhoA biosensors [59]. The CRIB domain of hsPAK1 is known to interact with GTP bound form of ROP [60,61]. We used it as a genetic probe for ROP6 GTP conformation. We ordered a synthetic gene coding for PAK1-mCherry-mVenus-ROP6 (iROP) and cloned it into *pDONR221*. The different binary were used either for transient expression in tobacco [62] or to generate stable Arabidopsis plants by floral dip method in Col-0 and then crossed with *rop6.2* line [63]. Additional information on all constructs vectors and oligonucleotides is provided in Table S2 and S3 respectively.

Osmotic and Pharmacological Treatments

Plantlets were bathed in a liquid MS/2 medium for 30 min to allow recovery from transplanting. When indicated, a pre-treatment with DPI (30min, 20µM), BPDS (50 µM, 30min), flg22 (1 µM, 30 min), ABA (1 µM, 1 hour), NAA (10µM, 1 hour) or H202 (1mM, 3mins for TIRF imaging and 1h for ligning quantification) was applied. Then, plantlets were gently transferred for an additional 15 min with 5 µM of ROS dye dehydroethidium (DHE) , with or without the corresponding inhibitors, into MS/2 medium (0 MPa), MS/2 medium plus 100 mM sorbitol (-0.26 MPa) for mild stress or MS/2 medium plus 300 mM sorbitol (-0.75 MPa) for severe osmotic stress. 300g/l PEG8000 was also used to mimic severe osmotic stress. The osmotic potential of each solution was verified by point freezing osmometer (WESCOR, VAPRO 5520).

Western blot

Tissues from 5 days old Col-0, *rop6.2*xmCit-ROP6g and GFP-ROP6 plantlets were grinded with liquid nitrogen to a fine powder and resuspended in 1 mL/g powder of RIPA extraction buffer (150 mM NaCl, 50mM Tris-HCl, pH- 8, 0.1% SDS, 0.5% Na deoxycholate, 1% Triton X-100, 2mM leupeptin, 1mM PMSF and 5mM DTT). Western blot analysis was performed with antibodies diluted in blocking solution (1% BSA in 0.1% Tween-20 and PBS) at the following dilutions: α-GFP with conjugated HRP 1:2000. Whole protein quantity was revealed with Commasie blue stain.

Sample clarification and phloroglucinol staining

Seedlings were vertically grown in half-strength MS-agar plates for 5 days and transfered on control (MS/2) or 300mM sorbitol plates for 24 hours. Plantlets were treated accordingly to Malamy et al., 1997 [64]. In brief, they were incubated in 0.24 M of HCl prepared in 20% ethanol, at 80°C for 15 minutes, and then transferred in a solution of 7% NaOH in 60% ethanol for another 15 minutes at room temperature. The incubated seedlings are rehydrated in subsequent baths for 5 minutes in 40%, 20% and 10% ethanol and infiltrated thereafter in 5% ethanol/25% glycerol for 15 minutes. Alternatively, root samples were stained with phloroglucinol as in Prajakta Mitra et al., 2014 [22].

ROS and autofluorescence quantification

Observations were performed on the root elongation zone using an Axiovert 200M inverted fluorescence microscope (20×/0.5 objective; Zeiss), with 512/25-nm excitation and 600/50 emission filters for DHE staining and with 475/28 nm excitation and 530/25 nm emission for lignin stained samples. Exposure time was 500 ms. Images were acquired using a CCD camera (Cooled SNAP HQ; PhotoMetrics), controlled by imaging software (MetaFluor; Molecular Devices). To quantify the intensity of the fluorescence signal, the images were analyzed using ImageJ software. After subtraction of the background noise, an average mean grey value was calculated from epidermal and cortical cells.

Confocal laser scanning microscopy

Signal from *rop6.2*xmCit-ROP6g, *rop6.2*xmCit-ROP6g-CA, *rop6.2*xmCit-ROP6g-DN and *rop6.2*xmCit-ROP6g$^{C21S/C158S}$ was imaged using Leica SP8 microscope with a 40×/1.1 water objective and the 488-nm line of its argon laser was used for live-cell imaging. Fluorescence emission was collected from 500–540 nm for GFP and from 600–650 nm by sequential acquisition when sample where stained 10 min with 2 µM of FM4-64. To detect FRET from the different iROP variants, images were taken with the 488-nm line of its argon laser and simultaneous detection between 515-540nm (mVenus detection) and 625-650nm (FRET channel). The ratio of FRET/Venus images was calculated with a Fiji software. Mean grey value of each cells present in the field of view was measured independently by drawing specific ROI.

TIRF microscopy

For cluster density analysis, Total Internal Reflection Fluorescence (TIRF) microscopy was done using an inverted Zeiss microscope and a 100x/1.45 oil immersion. Images were acquired with 50ms exposure time at 50 gain, with 475 nm excitation and 530/25 nm emission. Acquisitions were recorded for 0.5 seconds. Images were Z stacked by average intensity and object detection of GFP-ROP6, GFP-ROP6CA, RbohD-GFP and RbohF-GFP was made using machine learning-based segmentation with Elastik [65]. For colocalization study, TIRF microscopy was done using an inverted Nikon microscope (Eclipse) equipped with azimuthal-TIRFiLas2 system (Roper Scientific) and a 100x/1.49 oil immersion. One hundred images were acquired with 100ms exposure time using sequentially 488nm laser illumination with 425/20 emission filters and 561nm laser with 600/25.

FRET-FLIM

FRET-FLIM measurements were performed by multiphoton confocal microscopy (ZEISS LSM 780) with the method of measuring the lifetime of photons (TCSPC: Time correlated single photon counting) and under a 40x/1.3 oil immersion objective (Peter and Ameer-Beg, 2004). The GFP (donor GFP-RBOHD or GFP-RBOHF) was excited with 920 nm by a pulsating infra-red laser Ti:Saphir (Chameleon ULTRA II, COHERENT) during 90 seconds and the emitted fluorescence was collected by HPM-100 Hybrid detector. The decreasing fluorescence curve was obtained with the SPCImage (Becker-HIckl) software for each zone of interest. The lifetime of the GFP was estimated based on a regression curve, either mono-exponential when the donor was expressed alone and bi-exponential when the donor was expressed in the presence of the acceptor proteins (RFP-ROP6, RFP-ROP6-CA and RFP-ROP6-DN). Three biological repetitions were done and for every biological replicate, 5 cells were analyzed.

sptPALM

Root cells were observed with a homemade total internal reflection fluorescence microscope equipped with an electron-multiplying charge-coupled device camera (Andor iXON XU_897) and a 100×/1.45 oil immersion objective. The coverslips (Marienfeld 1.5H) were washed sequentially with 100% ethanol, acetone and water. Then, they were bathed with a 1M KOH solution and then ultra-soniccated for 30 min. After several wash-outs with MilliQ water, they were dried under Bunsen burner flame. The laser angle was adjusted so that the generation of the evanescence waves give a maximum signal-to-noise ratio. The activation of the photoconvertible tagged mEOS-ROP6, mEOS-ROP6-CA and mEOS-ROP6$^{C21A/C158S}$ was done by a low-intensity illumination at 405 nm (OBIS LX 50mW; Coherent), and 561 nm (SAPPHIRE 100mW; Coherent) emission combined with a 600/50 (Chroma) emission filter was used for image acquisition [12]. Ten-thousand images were recorded per region of interest and streamed into a LabVIEW software (National Instruments) at 20ms exposure time. Ten to 20 cells/ treatment were analysed out of three biological replicates.

Single-Particle Tracking and Vonoroi Tessellation

Individual single molecules were localized and tracked using the MTT software [66]. Dynamic properties of single emitters in root cells were then inferred from the tracks using a homemade analysis software written in MatLab (The MathWorks) [12]. From each track, the MSD was computed. To reduce the statistical noise while keeping a sufficiently high number of trajectories per cell, tracks of at least five steps (i.e. ≥ 6 localizations) were used. Missing frames due to mEOS blinking were allowed up to a maximum of three consecutive frames. The diffusion coefficient D was then calculated by fitting the MSD curve using the first four points. For the clustering analysis, the positions returned by MTT of each mEOS detection were used as input to the SR-Tesseler software [27]. Correction for multiple detection was made based on recommendation from Levet et al., 2015 [27]. The local densities of each track were calculated as the invert of their minimal surface. Then, nanocluster size, relative number of ROP6 molecules in nanodomains and density of nanoclusters were calculated after defining region of interest (ROI) where the local density was 50 times higher than the average. Only ROI with at least 25 detections were considered.

Statistical Analysis

For each condition or treatment, 9–12 cells were analyzed from at least 5–7 different seedlings. All experiments were independently repeated 2–3 times. Data are expressed as mean ± 95% confidence interval. ANOVA followed by Tukey test was done, letters indicate significant differences among means (pvalue<0.001). * p-value below 0.01 Student T-Test. Statistical analyses were performed in GraphPad Prism (GraphPad Software).

VIDEO S1 LEGEND

VIDEO S1: Dynamic of mEOS-ROP6 single molecule at the plasma membrane. Related to figure 2.

REFERENCES

1. Nicolson, G.L. (2014). The Fluid-Mosaic Model of Membrane Structure: still relevant to understanding the structure, function and dynamics of biological membranes after more than 40 years. Biochim. Biophys. Acta *1838*, 1451–1466.

2. Jaillais, Y., and Ott, T. (2020). The Nanoscale Organization of the Plasma Membrane and Its Importance in Signaling: A Proteolipid Perspective. Plant Physiol. *182*, 1682–1696.

3. Li, X., Wang, X., Yang, Y., Li, R., He, Q., Fang, X., Luu, D.-T., Maurel, C., and Lin, J. (2011). Single-molecule analysis of PIP2;1 dynamics and partitioning reveals multiple modes of Arabidopsis plasma membrane aquaporin regulation. Plant Cell *23*, 3780–3797.

4. Kleine-Vehn, J., Wabnik, K., Martinière, A., Łangowski, Ł., Willig, K., Naramoto, S., Leitner, J., Tanaka, H., Jakobs, S., Robert, S., *et al.* (2011). Recycling, clustering, and endocytosis jointly maintain PIN auxin carrier polarity at the plasma membrane. Mol. Syst. Biol. *7*, 540.

5. Wang, Q., Zhao, Y., Luo, W., Li, R., He, Q., Fang, X., Michele, R.D., Ast, C., von Wirén, N., and Lin, J. (2013). Single-particle analysis reveals shutoff control of the Arabidopsis ammonium transporter AMT1;3 by clustering and internalization. Proc. Natl. Acad. Sci. U. S. A. *110*, 13204–13209.

6. Martins, S., Dohmann, E.M.N., Dompierre, J., Fischer, W., Pojer, F., Jaillais, Y., Satiat-Jeunemaître, B., Chory, J., Geldner, N., and Vert, G. (2015). Dual role for ubiquitin in plant steroid hormone receptor endocytosis. Nat. Commun. *6*, 6151.

7. Hao, H., Fan, L., Chen, T., Li, R., Li, X., He, Q., Botella, M.A., and Lin, J. (2014). Clathrin and Membrane Microdomains Cooperatively Regulate RbohD Dynamics and Activity in Arabidopsis. Plant Cell *26*, 1729–1745.

8. Bücherl, C.A., Jarsch, I.K., Schudoma, C., Segonzac, C., Mbengue, M., Robatzek, S., MacLean, D., Ott, T., and Zipfel, C. (2017). Plant immune and growth receptors share common signalling components but localise to distinct plasma membrane nanodomains. eLife *6*, e25114.

9. Zhang, X., Cui, Y., Yu, M., Su, B., Gong, W., Baluška, F., Komis, G., Šamaj, J., Shan, X., and Lin, J. (2019). Phosphorylation-Mediated Dynamics of Nitrate Transceptor NRT1.1 Regulate Auxin Flux and Nitrate Signaling in Lateral Root Growth. Plant Physiol. *181*, 480–498.

10. Robbins, N.E., and Dinneny, J.R. (2015). The divining root: moisture-driven responses of roots at the micro- and macro-scale. J. Exp. Bot. *66*, 2145–2154.

11. Rui, Y., and Dinneny, J.R. A wall with integrity: surveillance and maintenance of the plant cell wall under stress. New Phytol. *n/a*. Available at: https://nph.onlinelibrary.wiley.com/doi/abs/10.1111/nph.16166 [Accessed November 7, 2019].

12. Martiniere, A., Fiche, J.B., Smokvarska, M., Mari, S., Alcon, C., Dumont, X., Hematy, K., Jaillais, Y., Nollmann, M., and Maurel, C. (2019). Osmotic stress activates two reactive oxygen species pathways with distinct effects on protein nanodomains and diffusion. Plant Physiol.

13. Boursiac, Y., Boudet, J., Postaire, O., Luu, D.-T., Tournaire-Roux, C., and Maurel, C. (2008). Stimulus-induced downregulation of root water transport involves reactive oxygen species-activated cell signalling and plasma membrane intrinsic protein internalization. Plant J. *56*, 207–218.

14. Ben Rejeb, K., Lefebvre-De Vos, D., Le Disquet, I., Leprince, A.-S., Bordenave, M., Maldiney, R., Jdey, A., Abdelly, C., and Savouré, A. (2015). Hydrogen peroxide

produced by NADPH oxidases increases proline accumulation during salt or mannitol stress in Arabidopsis thaliana. New Phytol. *208*, 1138–1148.

15. Feiguelman, G., Fu, Y., and Yalovsky, S. (2018). ROP GTPases Structure-Function and Signaling Pathways. Plant Physiol. *176*, 57–79.

16. Wong, H.L., Pinontoan, R., Hayashi, K., Tabata, R., Yaeno, T., Hasegawa, K., Kojima, C., Yoshioka, H., Iba, K., Kawasaki, T., *et al.* (2007). Regulation of rice NADPH oxidase by binding of Rac GTPase to its N-terminal extension. Plant Cell *19*, 4022–4034.

17. Sorek, N., Segev, O., Gutman, O., Bar, E., Richter, S., Poraty, L., Hirsch, J.A., Henis, Y.I., Lewinsohn, E., Jürgens, G., *et al.* (2010). An S-acylation switch of conserved G domain cysteines is required for polarity signaling by ROP GTPases. Curr. Biol. CB *20*, 914–920.

18. Nagano, M., Ishikawa, T., Fujiwara, M., Fukao, Y., Kawano, Y., Kawai-Yamada, M., and Shimamoto, K. (2016). Plasma Membrane Microdomains Are Essential for Rac1-RbohB/H-Mediated Immunity in Rice. Plant Cell *28*, 1966–1983.

19. Platre, M.P., Bayle, V., Armengot, L., Bareille, J., Marquès-Bueno, M.D.M., Creff, A., Maneta-Peyret, L., Fiche, J.-B., Nollmann, M., Miège, C., *et al.* (2019). Developmental control of plant Rho GTPase nano-organization by the lipid phosphatidylserine. Science *364*, 57–62.

20. Engelsdorf, T., Gigli-Bisceglia, N., Veerabagu, M., McKenna, J.F., Vaahtera, L., Augstein, F., Van der Does, D., Zipfel, C., and Hamann, T. (2018). The plant cell wall integrity maintenance and immune signaling systems cooperate to control stress responses in Arabidopsis thaliana. Sci. Signal. *11*.

21. Lee, Y., Rubio, M.C., Alassimone, J., and Geldner, N. (2013). A mechanism for localized lignin deposition in the endodermis. Cell *153*, 402–412.

22. Pradhan Mitra, P., and Loqué, D. (2014). Histochemical Staining of Arabidopsis thaliana Secondary Cell Wall Elements. J. Vis. Exp. JoVE. Available at: https://www.ncbi.nlm.nih.gov/pmc/articles/PMC4186213/ [Accessed October 28, 2019].

23. Vartanian, N., Marcotte, L., and Giraudat, J. (1994). Drought Rhizogenesis in Arabidopsis thaliana (Differential Responses of Hormonal Mutants). Plant Physiol. *104*, 761–767.

24. Geng, Y., Wu, R., Wee, C.W., Xie, F., Wei, X., Chan, P.M.Y., Tham, C., Duan, L., and Dinneny, J.R. (2013). A spatio-temporal understanding of growth regulation during the salt stress response in Arabidopsis. Plant Cell *25*, 2132–2154.

25. Hodge, R.G., and Ridley, A.J. (2016). Regulating Rho GTPases and their regulators. Nat. Rev. Mol. Cell Biol. *17*, 496–510.

26. Hosy, E., Martinière, A., Choquet, D., Maurel, C., and Luu, D.-T. (2015). Super-resolved and dynamic imaging of membrane proteins in plant cells reveal contrasting kinetic profiles and multiple confinement mechanisms. Mol. Plant *8*, 339–342.

27. Levet, F., Hosy, E., Kechkar, A., Butler, C., Beghin, A., Choquet, D., and Sibarita, J.-B. (2015). SR-Tesseler: a method to segment and quantify localization-based super-resolution microscopy data. Nat. Methods *12*, 1065–1071.

28. Zhai, L., Sun, C., Feng, Y., Li, D., Chai, X., Wang, L., Sun, Q., Zhang, G., Li, Y., Wu, T., *et al.* (2018). AtROP6 is involved in reactive oxygen species signaling in response to iron-deficiency stress in Arabidopsis thaliana. FEBS Lett. *592*, 3446–3459.

29. Lin, D., Nagawa, S., Chen, J., Cao, L., Chen, X., Xu, T., Li, H., Dhonukshe, P., Yamamuro, C., Friml, J., *et al.* (2012). A ROP GTPase-dependent auxin signaling pathway regulates the subcellular distribution of PIN2 in Arabidopsis roots. Curr. Biol. CB *22*, 1319–1325.

30. Chen, X., Naramoto, S., Robert, S., Tejos, R., Löfke, C., Lin, D., Yang, Z., and Friml, J. (2012). ABP1 and ROP6 GTPase signaling regulate clathrin-mediated endocytosis in Arabidopsis roots. Curr. Biol. CB *22*, 1326–1332.

31. Peer, W.A., Cheng, Y., and Murphy, A.S. (2013). Evidence of oxidative attenuation of auxin signalling. J. Exp. Bot. *64*, 2629–2639.

32. Mangano, S., Denita-Juarez, S.P., Choi, H.-S., Marzol, E., Hwang, Y., Ranocha, P., Velasquez, S.M., Borassi, C., Barberini, M.L., Aptekmann, A.A., *et al.* (2017). Molecular link between auxin and ROS-mediated polar growth. Proc. Natl. Acad. Sci. U. S. A. *114*, 5289–5294.

33. Krieger, G., Shkolnik, D., Miller, G., and Fromm, H. (2016). Reactive Oxygen Species Tune Root Tropic Responses. Plant Physiol. *172*, 1209–1220.

34. Duan, Q., Kita, D., Li, C., Cheung, A.Y., and Wu, H.-M. (2010). FERONIA receptor-like kinase regulates RHO GTPase signaling of root hair development. Proc. Natl. Acad. Sci. U. S. A. *107*, 17821–17826.

35. Fujita, S., De Bellis, D., Edel, K.H., Köster, P., Andersen, T.G., Schmid-Siegert, E., Dénervaud Tendon, V., Pfister, A., Marhavý, P., Ursache, R., *et al.* (2020). SCHENGEN receptor module drives localized ROS production and lignification in plant roots. EMBO J. *39*, e103894.

36. Pfister, A., Barberon, M., Alassimone, J., Kalmbach, L., Lee, Y., Vermeer, J.E.M., Yamazaki, M., Li, G., Maurel, C., Takano, J., *et al.* (2014). A receptor-like kinase mutant with absent endodermal diffusion barrier displays selective nutrient homeostasis defects. eLife *3*, e03115.

37. Wang, P., Calvo-Polanco, M., Reyt, G., Barberon, M., Champeyroux, C., Santoni, V., Maurel, C., Franke, R.B., Ljung, K., Novak, O., *et al.* (2019). Surveillance of cell wall diffusion barrier integrity modulates water and solute transport in plants. Sci. Rep. *9*, 4227.

38. Lin, D., Cao, L., Zhou, Z., Zhu, L., Ehrhardt, D., Yang, Z., and Fu, Y. (2013). Rho GTPase signaling activates microtubule severing to promote microtubule ordering in Arabidopsis. Curr. Biol. CB *23*, 290–297.

39. Remorino, A., Beco, S.D., Cayrac, F., Federico, F.D., Cornilleau, G., Gautreau, A., Parrini, M.C., Masson, J.-B., Dahan, M., and Coppey, M. (2017). Gradients of Rac1 Nanoclusters Support Spatial Patterns of Rac1 Signaling. Cell Rep. *21*, 1922–1935.

40. Abankwa, D., Gorfe, A.A., Inder, K., and Hancock, J.F. (2010). Ras membrane orientation and nanodomain localization generate isoform diversity. Proc. Natl. Acad. Sci. U. S. A. *107*, 1130–1135.

41. Sartorel, E., Ünlü, C., Jose, M., Massoni-Laporte, A., Meca, J., Sibarita, J.-B., and McCusker, D. (2018). Phosphatidylserine and GTPase activation control Cdc42 nanoclustering to counter dissipative diffusion. Mol. Biol. Cell *29*, 1299–1310.

42. Kadota, Y., Sklenar, J., Derbyshire, P., Stransfeld, L., Asai, S., Ntoukakis, V., Jones, J.D., Shirasu, K., Menke, F., Jones, A., *et al.* (2014). Direct regulation of the NADPH oxidase RBOHD by the PRR-associated kinase BIK1 during plant immunity. Mol. Cell *54*, 43–55.

43. Dubiella, U., Seybold, H., Durian, G., Komander, E., Lassig, R., Witte, C.-P., Schulze, W.X., and Romeis, T. (2013). Calcium-dependent protein kinase/NADPH oxidase activation circuit is required for rapid defense signal propagation. Proc. Natl. Acad. Sci. U. S. A. *110*, 8744–8749.

44. Keller, T., Damude, H.G., Werner, D., Doerner, P., Dixon, R.A., and Lamb, C. (1998). A plant homolog of the neutrophil NADPH oxidase gp91phox subunit gene encodes a plasma membrane protein with Ca2+ binding motifs. Plant Cell *10*, 255–266.

45. Ogasawara, Y., Kaya, H., Hiraoka, G., Yumoto, F., Kimura, S., Kadota, Y., Hishinuma, H., Senzaki, E., Yamagoe, S., Nagata, K., *et al.* (2008). Synergistic activation of the Arabidopsis NADPH oxidase AtrbohD by Ca2+ and phosphorylation. J. Biol. Chem. *283*, 8885–8892.

46. Means, S., Smith, A.J., Shepherd, J., Shadid, J., Fowler, J., Wojcikiewicz, R.J.H., Mazel, T., Smith, G.D., and Wilson, B.S. (2006). Reaction Diffusion Modeling of Calcium Dynamics with Realistic ER Geometry. Biophys. J. *91*, 537–557.

47. Oda, T., Hashimoto, H., Kuwabara, N., Akashi, S., Hayashi, K., Kojima, C., Wong, H.L., Kawasaki, T., Shimamoto, K., Sato, M., *et al.* (2010). Structure of the N-terminal Regulatory Domain of a Plant NADPH Oxidase and Its Functional Implications. J. Biol. Chem. *285*, 1435–1445.

48. Marhavý, P., Kurenda, A., Siddique, S., Dénervaud Tendon, V., Zhou, F., Holbein, J., Hasan, M.S., Grundler, F.M., Farmer, E.E., and Geldner, N. (2019). Single-cell damage elicits regional, nematode-restricting ethylene responses in roots. EMBO J. *38*.

49. Kang, E., Zheng, M., Zhang, Y., Yuan, M., Yalovsky, S., Zhu, L., and Fu, Y. (2017). The Microtubule-Associated Protein MAP18 Affects ROP2 GTPase Activity during Root Hair Growth. Plant Physiol. *174*, 202–222.

50. Fu, Y., Gu, Y., Zheng, Z., Wasteneys, G., and Yang, Z. (2005). Arabidopsis interdigitating cell growth requires two antagonistic pathways with opposing action on cell morphogenesis. Cell *120*, 687–700.

902 51. Ren, H., Dang, X., Yang, Y., Huang, D., Liu, M., Gao, X., and Lin, D. (2016). SPIKE1
903 Activates ROP GTPase to Modulate Petal Growth and Shape. Plant Physiol. *172*, 358–
904 371.

905 52. Veronese, P., Nakagami, H., Bluhm, B., Abuqamar, S., Chen, X., Salmeron, J., Dietrich,
906 R.A., Hirt, H., and Mengiste, T. (2006). The membrane-anchored BOTRYTIS-INDUCED
907 KINASE1 plays distinct roles in Arabidopsis resistance to necrotrophic and biotrophic
908 pathogens. Plant Cell *18*, 257–273.

909 53. Ranf, S., Eschen-Lippold, L., Fröhlich, K., Westphal, L., Scheel, D., and Lee, J. (2014).
910 Microbe-associated molecular pattern-induced calcium signaling requires the receptor-
911 like cytoplasmic kinases, PBL1 and BIK1. BMC Plant Biol. *14*, 374.

912 54. Boudsocq, M., Willmann, M.R., McCormack, M., Lee, H., Shan, L., He, P., Bush, J.,
913 Cheng, S.-H., and Sheen, J. (2010). Differential innate immune signalling via Ca(2+)
914 sensor protein kinases. Nature *464*, 418–422.

915 55. Mustilli, A.-C., Merlot, S., Vavasseur, A., Fenzi, F., and Giraudat, J. (2002). Arabidopsis
916 OST1 protein kinase mediates the regulation of stomatal aperture by abscisic acid and acts
917 upstream of reactive oxygen species production. Plant Cell *14*, 3089–3099.

918 56. Jaillais, Y., Hothorn, M., Belkhadir, Y., Dabi, T., Nimchuk, Z.L., Meyerowitz, E.M., and
919 Chory, J. (2011). Tyrosine phosphorylation controls brassinosteroid receptor activation by
920 triggering membrane release of its kinase inhibitor. Genes Dev. *25*, 232–237.

921 57. Karimi, M., Bleys, A., Vanderhaeghen, R., and Hilson, P. (2007). Building Blocks for
922 Plant Gene Assembly. Plant Physiol. *145*, 1183–1191.

923 58. Marquès-Bueno, M.D.M., Morao, A.K., Cayrel, A., Platre, M.P., Barberon, M., Caillieux,
924 E., Colot, V., Jaillais, Y., Roudier, F., and Vert, G. (2016). A versatile Multisite Gateway-
925 compatible promoter and transgenic line collection for cell type-specific functional
926 genomics in Arabidopsis. Plant J. Cell Mol. Biol. *85*, 320–333.

927 59. Pertz, O., Hodgson, L., Klemke, R.L., and Hahn, K.M. (2006). Spatiotemporal dynamics
928 of RhoA activity in migrating cells. Nature *440*, 1069–1072.

929 60. Tao, L., Cheung, A.Y., and Wu, H. (2002). Plant Rac-like GTPases are activated by auxin
930 and mediate auxin-responsive gene expression. Plant Cell *14*, 2745–2760.

931 61. Akamatsu, A., Wong, H.L., Fujiwara, M., Okuda, J., Nishide, K., Uno, K., Imai, K.,
932 Umemura, K., Kawasaki, T., Kawano, Y., *et al.* (2013). An OsCEBiP/OsCERK1-
933 OsRacGEF1-OsRac1 module is an essential early component of chitin-induced rice
934 immunity. Cell Host Microbe *13*, 465–476.

935 62. Sparkes, I.A., Runions, J., Kearns, A., and Hawes, C. (2006). Rapid, transient expression
936 of fluorescent fusion proteins in tobacco plants and generation of stably transformed
937 plants. Nat. Protoc. *1*, 2019–2025.

938 63. Clough, S.J., and Bent, A.F. (1998). Floral dip: a simplified method for Agrobacterium-
939 mediated transformation of Arabidopsis thaliana. Plant J. Cell Mol. Biol. *16*, 735–743.

64. Malamy, J.E., and Benfey, P.N. (1997). Organization and cell differentiation in lateral roots of Arabidopsis thaliana. Dev. Camb. Engl. *124*, 33–44.

65. Berg, S., Kutra, D., Kroeger, T., Straehle, C.N., Kausler, B.X., Haubold, C., Schiegg, M., Ales, J., Beier, T., Rudy, M., *et al.* (2019). ilastik: interactive machine learning for (bio)image analysis. Nat. Methods, 1–7.

66. Sergé, A., Bertaux, N., Rigneault, H., and Marguet, D. (2008). Dynamic multiple-target tracing to probe spatiotemporal cartography of cell membranes. Nat. Methods *5*, 687–694.

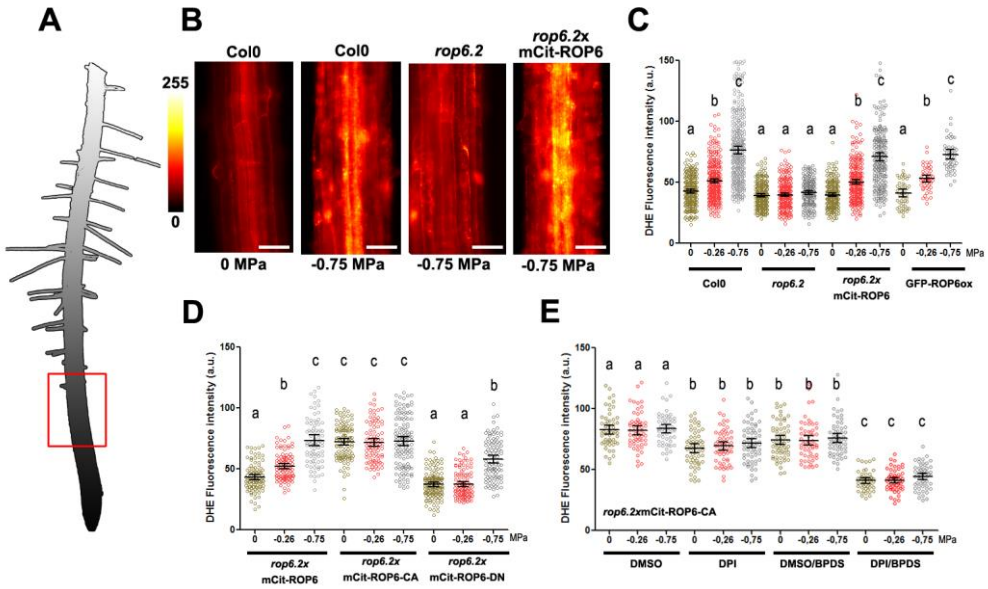

Figure 1: ROP6 activation is necessary and sufficient to trigger osmotically driven ROS accumulation in Arabidopsis root cells. (A) Drawing of Arabidopsis plantlets, where the red square highlights the part of root under study. (B) Dihydroethidium (DHE) stained root cell of Col0, *rop6.2* and *rop6.2*xmCit-ROP6 in control condition (0 MPa) or after 15 min of -0.75 MPa treatment. (C-D) DHE fluorescence quantification after 15 min treatment with 0, -0.26 or -0.75 MPa solution in different genetic materials: Col(0), *rop6.2*, ROP6 over expresser line (GFP-ROP6ox) and *rop6.2* lines expressing under ROP6 endogenous promotor, either ROP6 (mCit-ROP6 (*rop6.2*xmCit-ROP6), the constitutive active ROP6 (*rop6.2*xmCit-ROP6-CA) or the dominant negative (*rop6.2*xmCit-ROP6-DN). (E) ROS quantification (DHE fluorescence) in root cells expressing the constitutive active ROP6 (mCit-ROP6-CA) in control or after mild or high osmotic stimulus (respectively 0, -0.26 and -0.75 MPa) supplemented or not with ROS enzyme inhibitors. DPI was used for inhibition of NADPH oxidase activity and BPDS to inhibit ROS produced from ferric iron. Error bars correspond to a confidence interval at 95%. ANOVA followed by Tukey test, letters indicate significant differences among means (p-value<0.001). n>49 from 4-6 independent biological replicates. Scale bar 20 µm.

See also Figure S1, S2 and S3.

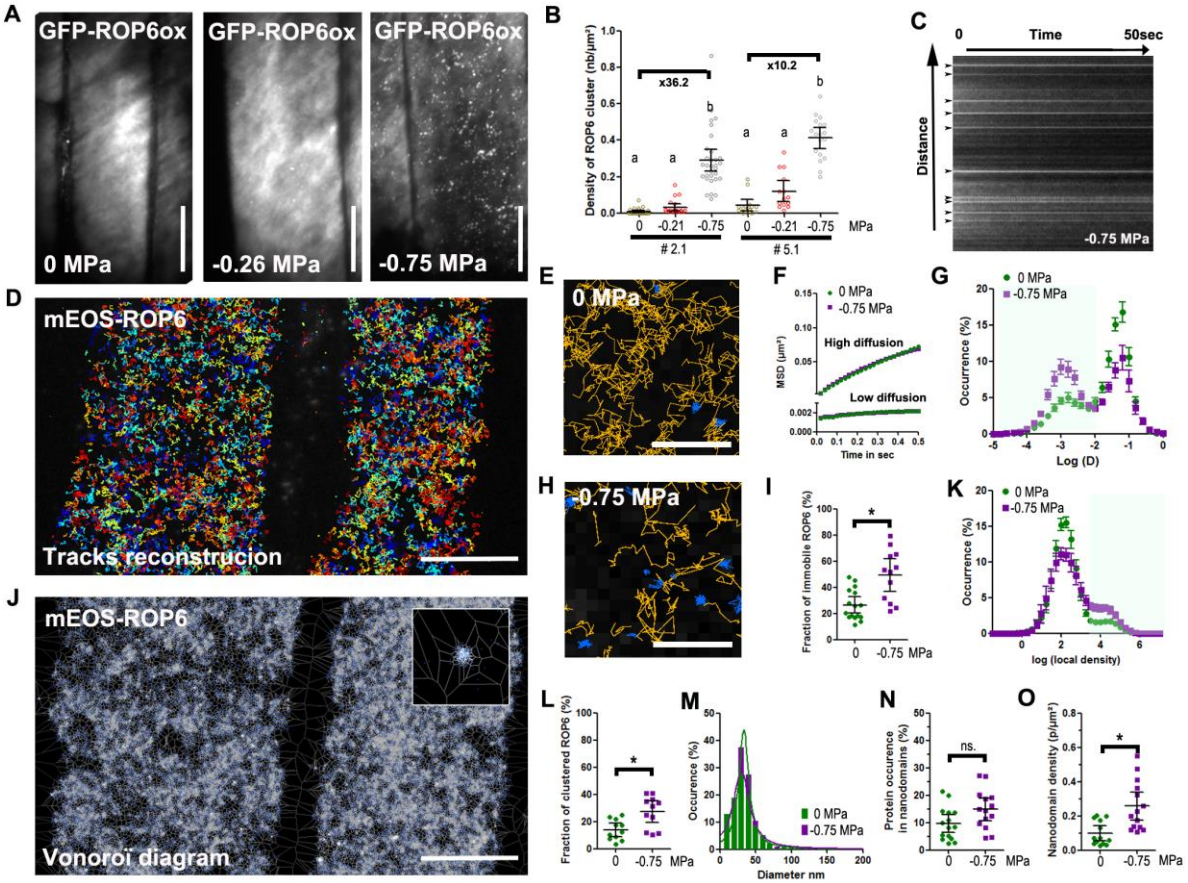

Figure 2: Osmotic stimulus triggers ROP6 molecular nanoclustering at the PM
(A) TIRFM micrograph of oxGFP-ROP6 expressing cells after 2 min incubation with solutions at either 0 MPa, -0.26 or -0.75 MPa. (B) Quantification of ROP6 cluster density. (C) Kymograph image of oxGFP-ROP6 clusters from cells exposed to 0.75 MPa. Clusters at initial time point are labelled with arrows. (D) Image reconstruction of around 5 000 single mEOS2-ROP6 molecule trajectories in two control cells. (E) Close-up view of cell expressing mEOS2-ROP6, where trajectories with high or low diffusion instantaneous coefficient labelled in orange or blue respectively. (F) Mean square displacement curves of the highly or lowly diffusible molecules in control (0 MPa) or treatment (-0.75 MPa) conditions. (G) Bimodal distribution of molecule instantaneous diffusion coefficients in control (0 MPa, green curve) and treatment (-0.75 MPa, purple curve) conditions. (H) Close up view of the PM of cells expressing mEOS2-ROP6 2 minutes after a -0.75 MPa treatment. (I) Histogram represents the percentage of molecules with an instantaneous diffusion below 0.01 $um^2.s^{-1}$ in control (0 MPa) or after treatment (-0.75 MPa). (J) Vonoroï tessellation of mEOS2-ROP6 molecules localization map from the exact same two control cells of (D). Top right inset is a close up view, showing a mEOS2-ROP6 nanodomain. (K) Distribution of molecules local density in control (0 MPa, green curve) and treatment (-0.75 MPa, purple curve) conditions. (L) Percentage of molecules with a log(local density) higher than 3. (M) Distribution of the mEOS2-ROP6 nanodomains diameter in control (0 MPa) and treatment (-0.75 MPa) conditions. (N) Relative occurrence of mEOS2-ROP6 in nanodomains in control (0 MPa) and treatment (-0.75 MPa) conditions. (O) Nanodomain density in control (0 MPa) or after 2 minutes treatment with -0.75 MPa solution. Error bars correspond to a confidence interval at 95%. For (B) an ANOVA followed by Tukey test was done, letters indicate significant differences among

means (p-value<0.001). * p-value below 0.01 T-Test. n>12 from 3 independent biological replicates. Scale Bar 10μm, except for E and H where it is 1 μm.

See also Figure S3, S4 and Video S1

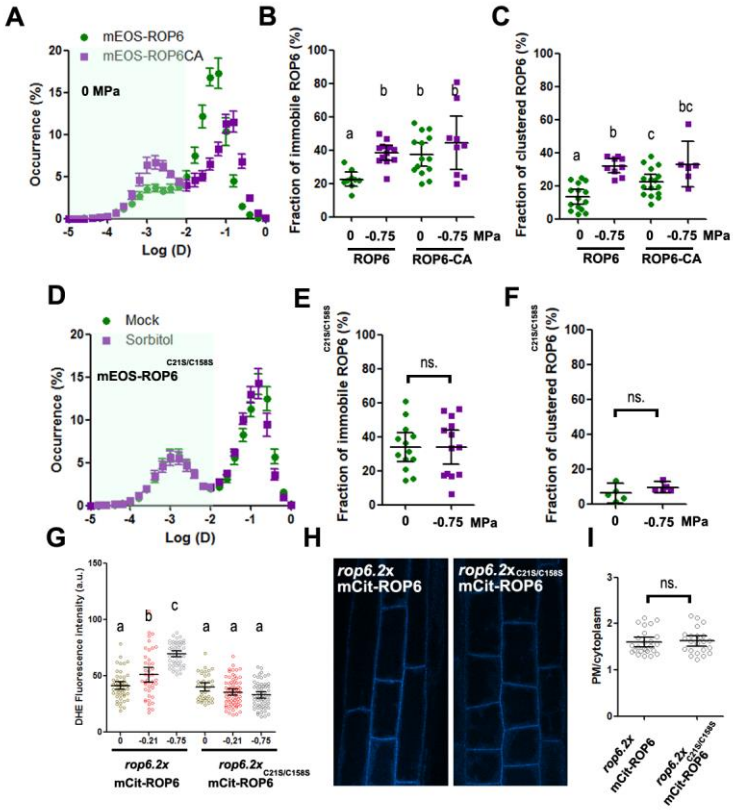

Figure 3: ROP6 nanoclustering is required for ROS accumulation. (A) Bimodal distribution of mEOS2-ROP6 instantaneous diffusion (green curve) or mEOS2-ROP6-CA (purple curve) in control condition (0 MPa). (B) Histogram represents the percentage of molecules with an instantaneous diffusion below 0.01 $um^2.s^{-1}$ in mEOS2-ROP6 and mEOS2-ROP6-CA expressing lines in control (green) or after osmotic stimulation (purple). (C) Percentage of molecules with a log(local density) higher than 3 in mEOS2-ROP6 and mEOS2-ROP6-CA expressing lines in control (green) or after osmotic stimulation (purple). (D) Bimodal distribution of mEOS2-ROP6$^{C21S/C158S}$ instantaneous diffusion coefficients in control (0 MPa, green curve) and treatment (-0.75 MPa, purple curve) conditions. (E) Histogram represents the percentage of mEOS2-ROP6$^{C21S/C158S}$ molecules with an instantaneous diffusion below 0.01 $um^2.s^{-1}$ in control (0 MPa) and treatment (-0.75 MPa) conditions. (F) Percentage of mEOS2-ROP6$^{C21S/C158S}$ molecules with a log(local density) higher than 3. (G) Quantification of ROS accumulation by DHE staining in *rop6.2*xmCit-ROP6 or *rop6.2*xmCit-ROP6$^{C21S/C158S}$ expressing cells after 15 min treatment with 0, -0.26 or -0.75 MPa solution. (H) Plasma membrane localization of mCit-ROP6 and mCit-ROP6$^{C21S/C158S}$ and its relative amount at the PM (I). Error bars correspond to a confidence interval at 95%. * p-value below 0.01 *t*-test. ns. Non-significant. n>9 from 3 independent biological replicates. Scale bar 10µm.

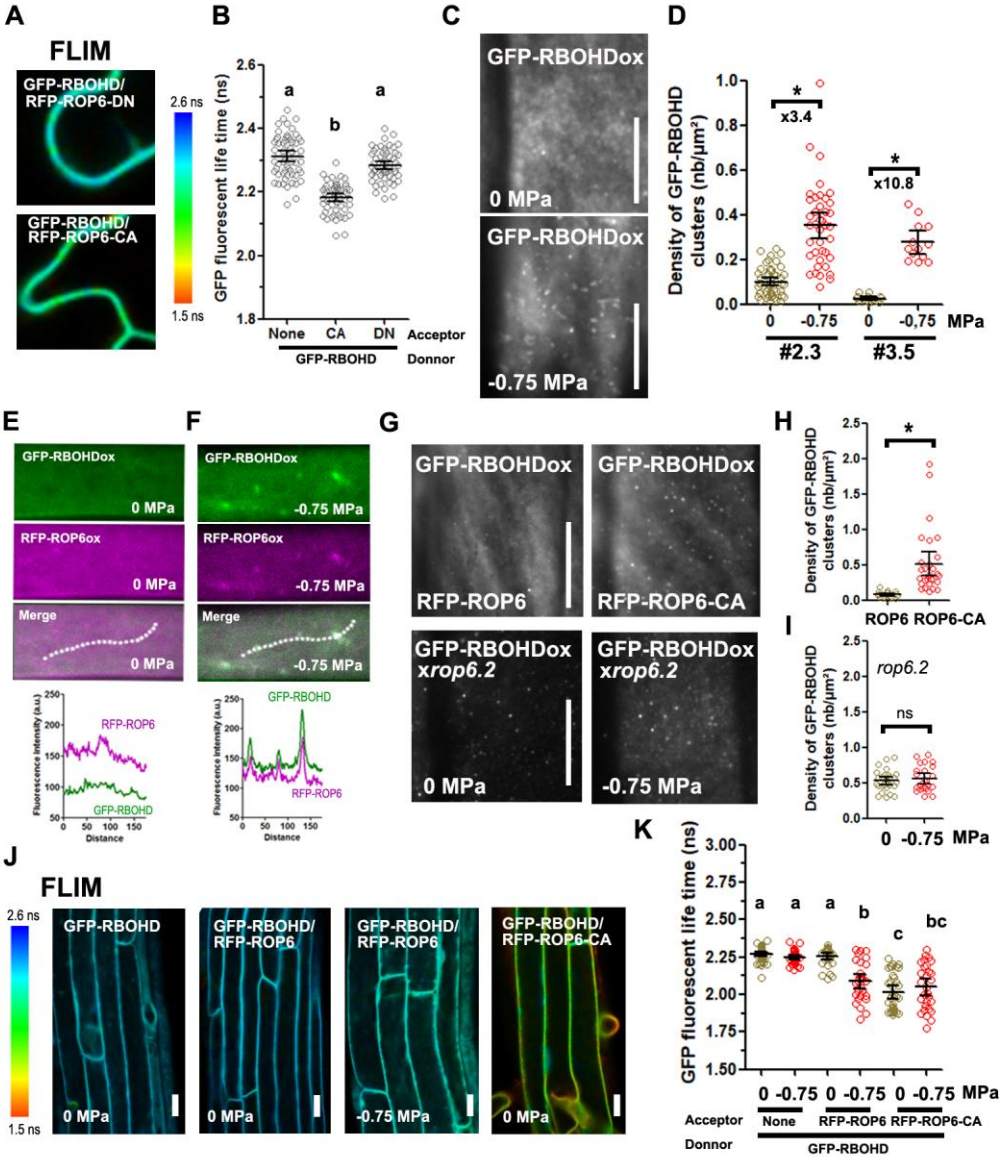

Figure 4: ROP6 interacts and forms nanoclusters with RBOHD at the PM. (A) GFP-RBOHD fluorescence lifetime when co-expressed with dominant negative (RFP-ROP6-DN) or constitutive active ROP6 (RFP-ROP6-CA) in transient expression in tobacco leaf epidermal cells and its quantification (B). (C) TIRF micrograph of cell expressing GFP-RBOHD in control or after 2 minute treatment with -0.75 MPa solution and quantification of clusters density (D). (E, F) Cell co-expressing GFP-RBOHD with RFP-ROP6 in control (E) or after -0.75 MPa treatment (F). Graphs below represent the pixel intensity along the dotted line in each of the conditions. (G) TIRFM micrograph of GFP-RBOHD signal in GFP-RBOHDxRFP-ROP6, GFP-RBOHDxRFP-ROP6-CA and *rop6.2*xGFP-RBOHD plant in control or after -0,75 MPa incubation and their respective quantification (H and I). (J) GFP-RBOHD fluorescence lifetime when expressed alone or co-expressed with RFP-ROP6 or RFP-ROP6-CA in root cells and its quantification (K). Error bars correspond to a confidence interval at 95%. For (B) an ANOVA followed by Tukey test was done, letters indicate significant differences among means (p-value<0.001). * p-value below 0.01 T-Test. n>12 from 3 independent biological replicates. Scale bar 10µm.

See also Figure S5

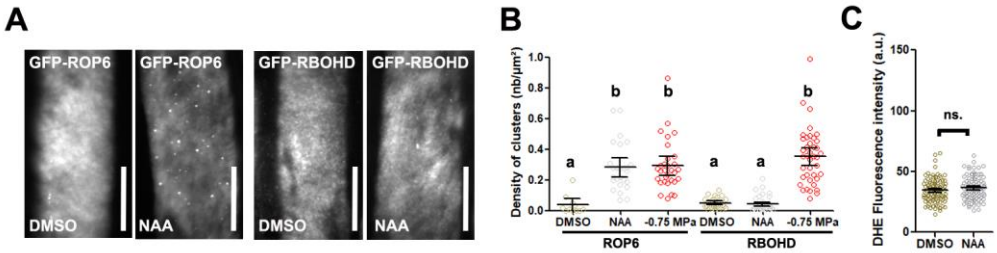

Figure 5: Auxin-stimulated ROP6 nanodomains are free of RBOHD. (A) TIRFM micrograph of cell expressing GFP-ROP6 or GFP-RBOHD in control condition (DMSO) or after 10 µM NAA for 1 hour. (B) Cluster density quantification after NAA or -0,75 MPa treatment. (C) Quantification of ROS accumulation by DHE staining in control (DMSO) or after 15 min treatment with 10 µM NAA. Error bars correspond to a confidence interval at 95%. For (B) an ANOVA followed by Tukey test was done, letters indicate significant differences among means (p-value<0.001). * p-value below 0.01 T-Test. n>11 from 3 independent biological replicates. Scale bar 10µm.

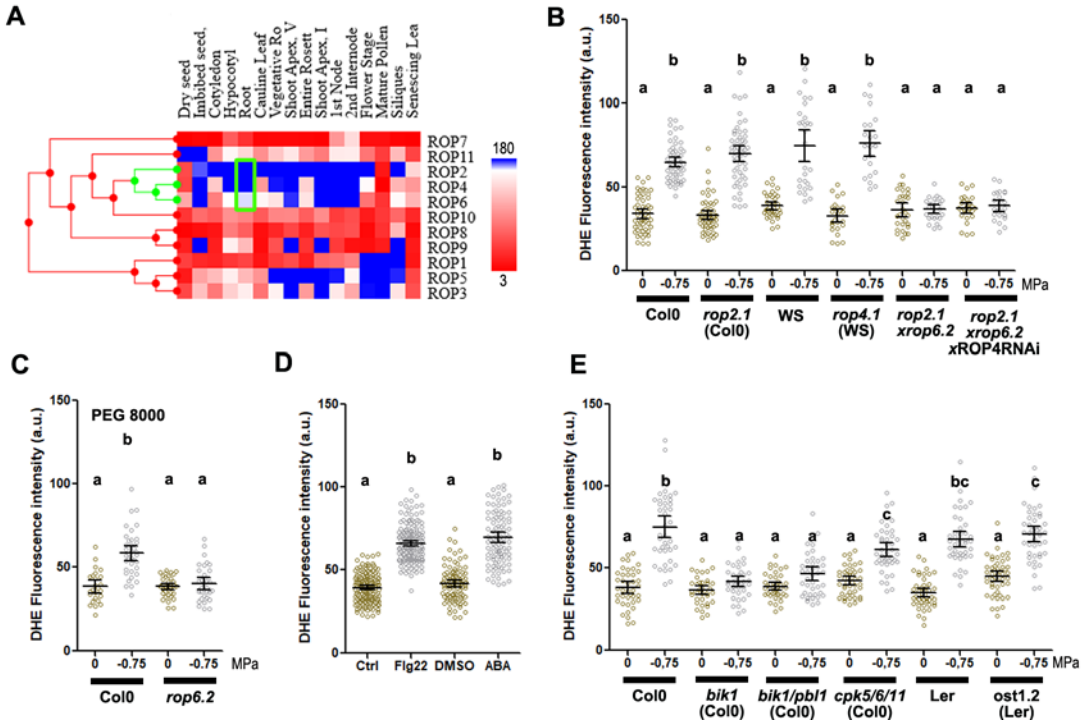

Figure S1: Expression pattern of different *ROP* isoforms and ROS production phenotypes of single and multiple mutants. Related to Figure 1.

(A) Gene expression clustering of the different ROP isoforms based on eFP-browser databases. Green square shows the three isoform highly expressed in root tissue (*ROP2*, *ROP4* and *ROP6*). (B-E) Quantification of ROS accumulation (DHE staining) in control or after 15 minutes of -0.75 MPa treatment in the indicated genotype, with either sorbitol (B and E), PEG8000 (C), or with 1 µM flg22 fro 30 minutes (D) or 1 µM of ABA for 1 hour (D). Error bars correspond to a confidence interval at 95%. ANOVA followed by Tukey test was done, letters indicate significant differences among means (p-value<0.001). n>21 from at least 2 independent biological replicates.

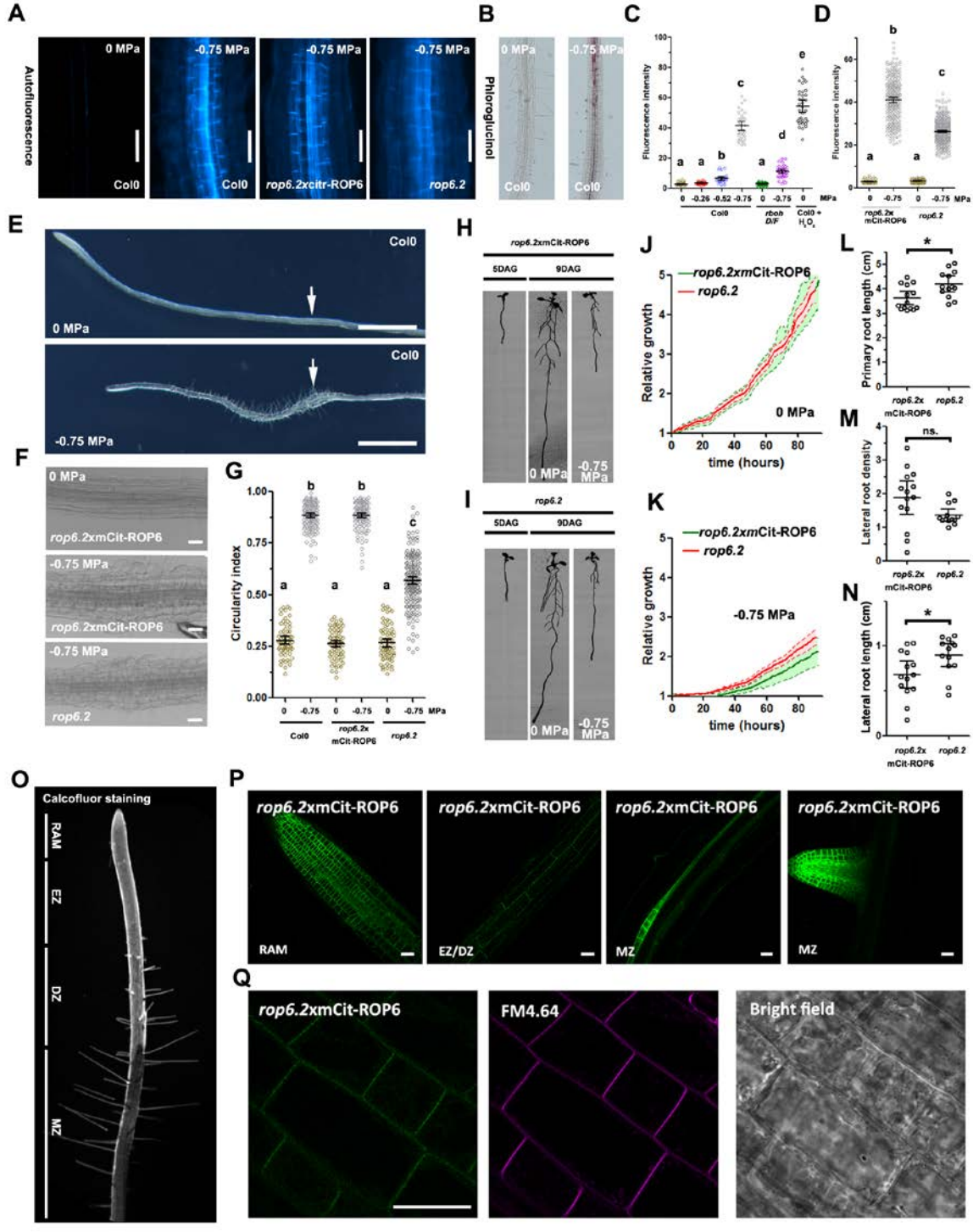
A
Autofluorescence
0 MPa
-0.75 MPa
-0.75 MPa
-0.75 MPa
Col0
Col0
rop6.2xcitr-ROP6
rop6.2
B
Phloroglucinol
0 MPa
-0.75 MPa
Col0
Col0
C
Fluorescence intensity
0 -0.26 -0.52 -0.75 0 -0.75 0 MPa
Col0
rboh D/F
Col0 + H2O2
D
Fluorescence intensity
0 -0.75 0 -0.75 MPa
rop6.2x mCit-ROP6
rop6.2
E
Col0
0 MPa
Col0
-0.75 MPa
F
0 MPa
rop6.2xmCit-ROP6
-0.75 MPa
rop6.2xmCit-ROP6
-0.75 MPa
rop6.2
G
Circularity index
0 -0.75 0 -0.75 0 -0.75 MPa
Col0
rop6.2x mCit-ROP6
rop6.2
H
rop6.2xmCit-ROP6
5DAG
9DAG
0 MPa
-0.75 MPa
I
rop6.2
5DAG
9DAG
0 MPa
-0.75 MPa
J
rop6.2xmCit-ROP6
rop6.2
Relative growth
0 MPa
time (hours)
K
rop6.2xmCit-ROP6
rop6.2
Relative growth
-0.75 MPa
time (hours)
L
Primary root length (cm)
rop6.2x mCit-ROP6
rop6.2
M
Lateral root density
ns.
rop6.2x mCit-ROP6
rop6.2
N
Lateral root length (cm)
rop6.2x mCit-ROP6
rop6.2
O
Calcofluor staining
RAM
EZ
DZ
MZ
P
rop6.2xmCit-ROP6
RAM
rop6.2xmCit-ROP6
EZ/DZ
rop6.2xmCit-ROP6
MZ
rop6.2xmCit-ROP6
MZ
Q
rop6.2xmCit-ROP6
FM4.64
Bright field

Figure S2: Expression pattern and implication of ROP6 in plant responses to osmotic stimulus. Related to Figure 1.

(A) Cell autofluorescence of *rop6.2* and complemented lines expressing mCit-ROP6 under ROP6 endogenous promotor in control plate or after -0.75 MPa treatment for 24 hours. (B) Phloroglucinol staining, that shows pink precipitates when in complex with lignin in control condition or after -0.75 MPa treatment for 24 hours. (C) Cell autofluorescence quantification of Col-0 plant exposed for 24 hours to control, -0.26, -0.5, -0.75 MPa. As a comparison, cell autofluorescence was also observed in *rbohDxrbohF* line exposed to -0.75 MPa and Col-0 treated for 1 hour with 1mM H_2O_2. (D) Cell autofluorescence quantification in *rop6.2* and *rop6.2*xmCit-ROP6 in control or treated (-0.75 MPa) conditions. (E) 2 days after transfer on -0.75 MPa plate, root cells present inflated cells (arrow). The arrows are located at the point where the root tip was at the time of transfer. (F) Close up view of cells in this zone in control condition or after treatment (-0.75 MPa) for *rop6.2*xmCit-ROP6 or *rop6.2*. (G) Quantification of cell circularity index. (H-N) the complemented line (*rop6.2*xmCit-ROP6) or the mutant *rop6.2* were grown 5 days on control plates and then transferred for 4 more days in either control condition or on plate supplemented with osmoticum to reach -0.75 MPa. Relative growth of *rop6.2*xmCit-ROP6 or *rop6.2* in control (J) or in -0.75 MPa plate (K). Quantification of the primary root length (L), lateral density (M) and lateral root length (N) of *rop6.2*xmCit-ROP6 or *rop6.2* grown on -0.75 MPa plates. (O) Arabidopsis control plant counterstained with calcofluor bright to illustrate the different root zone. Root apical meristem (RAM), elongation zone (EZ), differentiation zone (DZ) and mature zone (MS). (P) Representative micrograph of the fluorescent signal observed in *rop6.2* lines complemented with mCit-ROP6 under ROP6 endogenous promoter. (Q) mCit-ROP6 signal is mostly visible at the cell PM, as revealed by FM4-64 staining. Error bars correspond to a confidence interval at 95%. ANOVA followed by Tukey test was done, letters indicate significant differences among means (p value <0.001). Scale bar 20µm for (A, F, P and Q), 2 mm for (E). n>14 from 3 independent biological replicates.

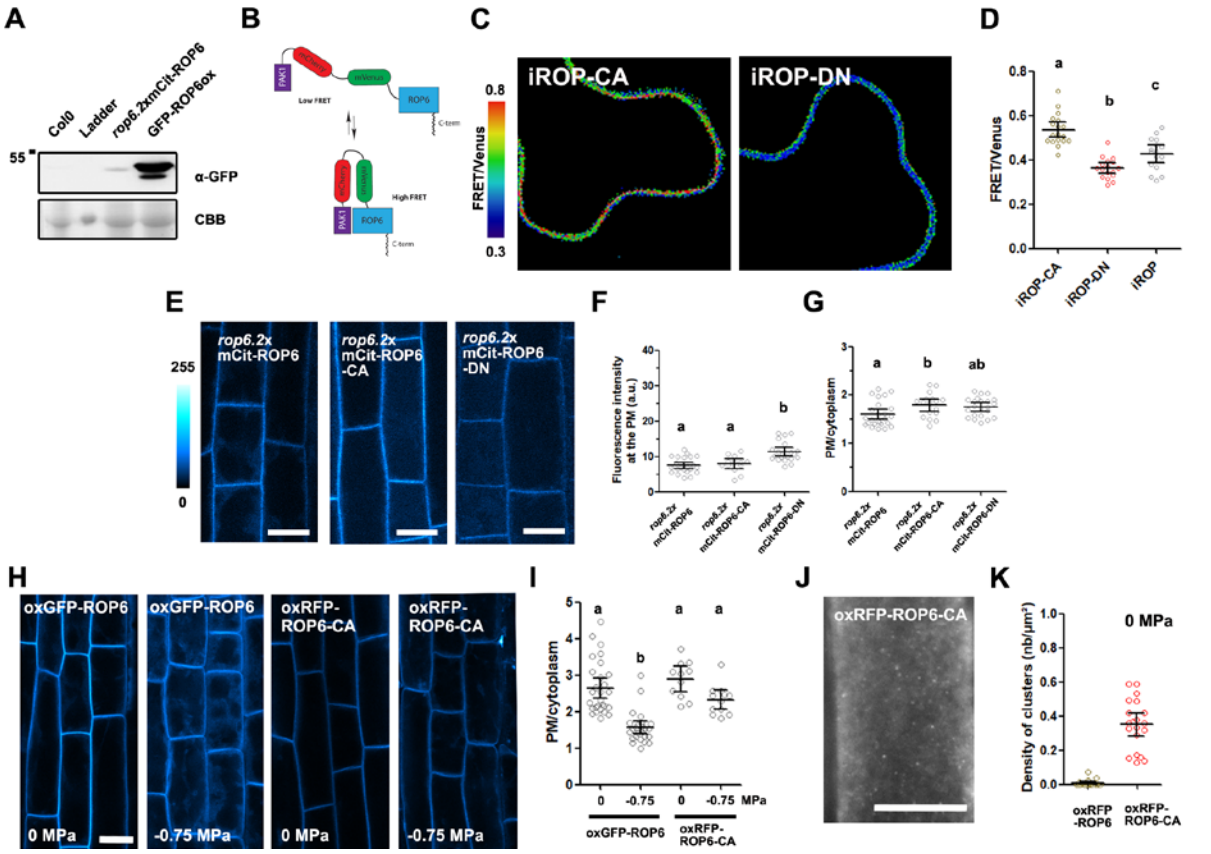

Figure S3: Characterization of GFP-ROP6 overexpressing line, detection of ROP6 activation with iROP sensor and localization of *rop6.2*xmCit-ROP6, *rop6.2*xmCit-ROP6-CA and *rop6.2*xmCit-ROP6-DN. Related to Figure 1 and 2.

(A) Western blot with antibody against GFP on plant protein extract from Col-0, ROP6 complemented line (*rop6.2*xmCit-ROP6) and ROP6 overexpressing line (oxGFP-ROP6). (B) Schematic view of iROP sensor. GTP-bound form of ROP6 interacts with PAK1, allowing FRET between Venus and mCherry. In contrast, if ROP6 is inactive in its GDP-bound form the distance between the two fluorescent proteins increases, thereby diminishing FRET efficiency. (C) Ratio images of transient expression of iROP sensors locked in GTP form (iROP-CA) or in GDP form (iROP-DN). (D) Relative variation of FRET between iROP-CA, iROP-DN and iROP. (E) Confocal micrograph showing the localization of wild type ROP6 (mCit-ROP6), constitutive active ROP6 (mCit-ROP6-CA) and dominant negative ROP6 (mCit-ROP6-DN).(F,G) Respective fluorescence (F) and relative amount at the PM (G) of the same forms. (H) Confocal micrograph showing the localization of oxGFP-ROP6 and oxRFP-ROP6-CA in control condition and after -0.75 MPa treatment and its respective quantification (I). (J) TIRFM micrograph of oxGFP-ROP6-CA expressing cells. (K) Quantification of clusters density of oxGFP-ROP6 and oxRFP-ROP6-CA in control condition. CBB, Coomassie brilliant blue. n>11 from at least 2 independent biological replicates. Scale bar 10µM.

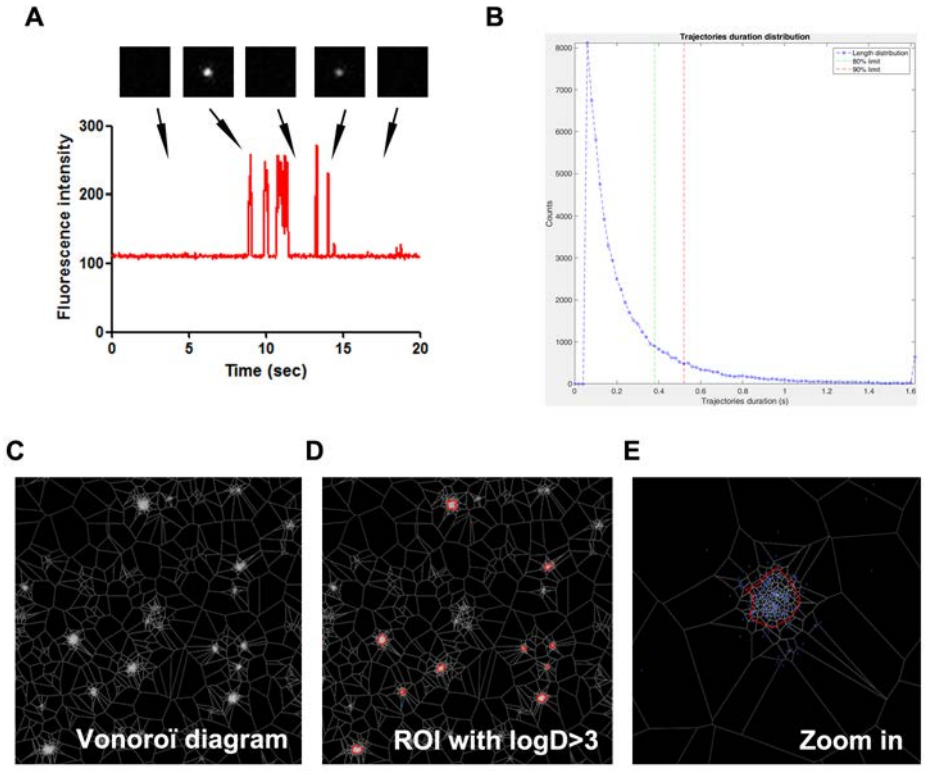

Figure S4: ROP6 single-molecule imaging and Vonoroï tessellation. Related to Figure 2

(A) To verify that we are indeed recording single mEOS2-ROP6 molecules, we plot fluorescence intensity of a typical mEOS2-ROP6 sub-diffractive cluster along time. The signal intensity observed is not continuous and the OFF state vary in duration between seconds and milliseconds. This blinking behaviour is typical from single-molecule observation. We also quantify the track duration (B). As expected from single molecules, vast majority of the tracks do not last for more than 0.5 seconds. (C) Picture of Vonoroï diagram, where each point/seeds corresponds to a mEOS2-ROP6 localization and edges of Vonoroï cells are represented in white. (D) Segmented region of interest (ROI) with a particle local density greater than log (local density)>3 (ROI appear in red). (E) Close up view of a ROP6 nanodomain where each blue dot represents one mEOS2-ROP6 localization.

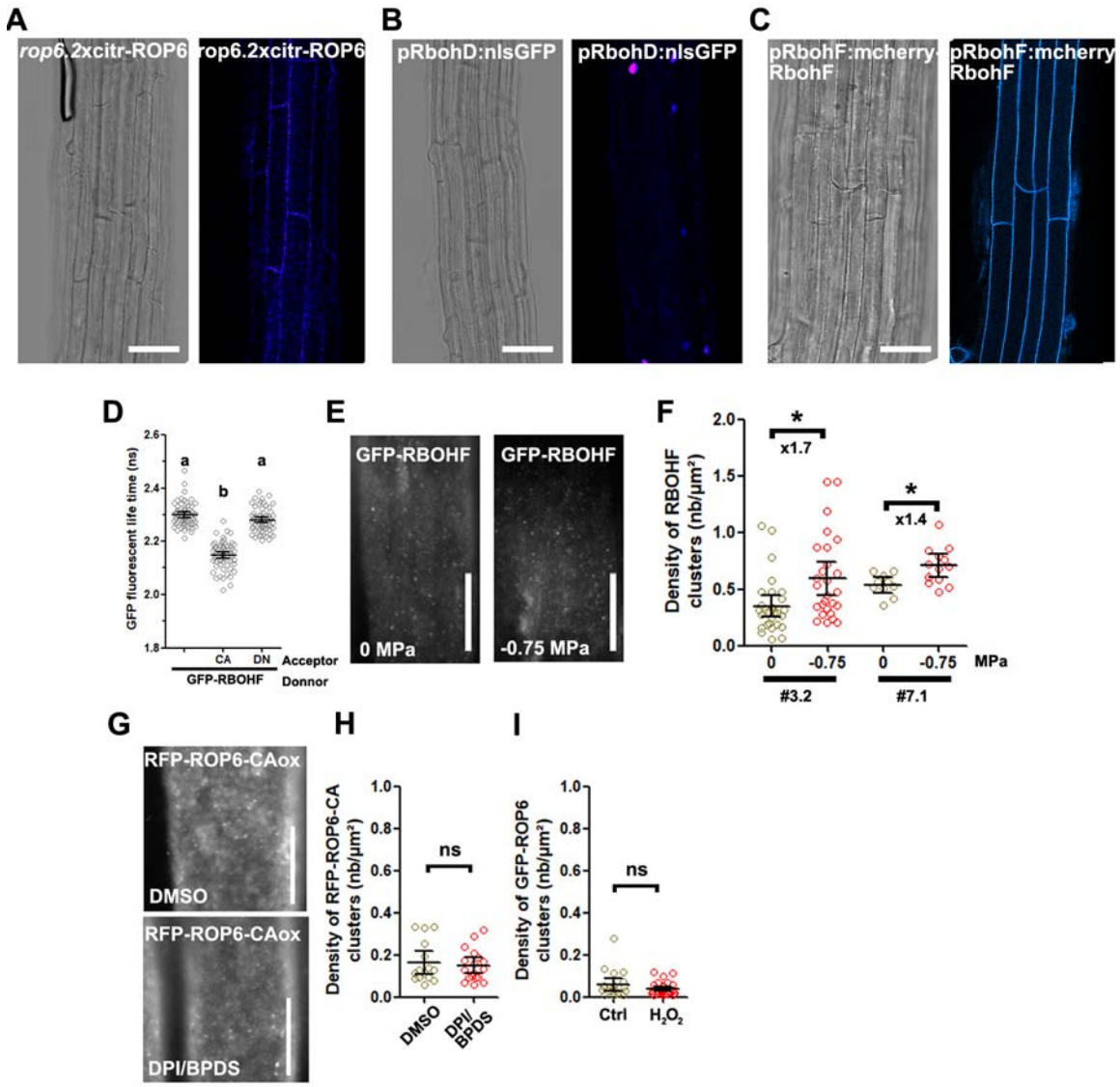

Figure S5: ROP6, RBOHD and RBOHF expression pattern, interaction and cluster formation. Related to Figure 4.

Expression pattern of the translational fusion pROP6:mCit-ROP6 (A) and pRBOHF:mCherry-RBOHF (B) and the transcriptional fusion pRBOHD:nls-GFP-GUS (C). (D) Quantification of GFP-RBOHF fluorescence life time expressed in transient expression in tobacco leaf epidermal cells, either alone, or co-expressed with the dominant negative (RFP-ROP6-DN) or the constitutive active ROP6 (RFP-ROP6-CA). (E) TIRFM micrograph of cell expressing GFP-RBOHF in control or after 2 minutes treatment with -0.75 MPa solution and quantification of cluster density (F). (G) TIRFM micrograph of RFP-ROP6-CA signal in control condition or after incubation for 30 min with ROS inhibitors and it is quantification (H). DPI was used for inhibition of NADPH oxidase activity and BPDS was

used to inhibit ROS produced from ferric iron. (I) Quantification in GFP-ROP6 cluster density in control condition or after H_2O_2 treatment. Error bars correspond to a confidence interval at 95%. For (D and F), ANOVA followed by Tukey test was done, letters indicate significant differences among means (p-value<0.001). ns: p-value above 0.05 T-Test. n>9 from 3 independent biological replicates. Scale bar 5µm for A, B and C and 10µm for E and G.

Gene	Gene-ID	Mutant allele	Ecotype	Mutant ID
ROP6	At4g35020	*rop6-2*	Col-0	SALK_ 091737C [29]
ROP2	At1g20090	*rop2-1*	Col-0	SALK_055328 [49]
ROP4	At1g75840	*rop4-1*	WS	Wisconsin T-DNA line [50]
		rop6-2xrop2-1	Col-0	crossing parental single homozygous lines [51]
		rop6-2xrop2-1 xROP4RNAi	Col-0	ROP4-RNAi was added on double homozigous rop2-1 and rop6-2 line [51]
BIK1	At2g39660	*bik1*	Col-0	SALK_005291 [52]
PBL1	At3g55450			
		bik1xpbl1	Col-0	*cross between bik1* (from Veronese et al., 2006) and SAIL_1236_D07 lines [53]
CPK5	At4g35310			
CPK6	At2g17290			
CPK10	At1g18890			
		cpk5/6/11	Col-0	cpk5:Sail_657C06 from Syngenta; cpk6:salk_025460; cpk11:salk_054495 [54]
OST1	At4g33950	*ost1-1*	Ler	EMS II-52, II-56, II-123 [55]
RBOHD	AT5G47910			
RBOHF	AT1G64060			

Table S1. List of identifiers for genes and single mutant alleles used in this study. Related to Star Methods

Gateway expression vectors	Promoter	N-terminal Tag	ORF / CDS	C-terminal Tag	Plant selection marker	Bacterial selection marker	Binary vector
pROP6:mCit-ROP6g-CA	ROP6-Promoter	mCitrine vo STOP	mutated (G15V) ROP6 genomic sequence	/	Basta	Kana	pB7m34GW
pROP6:mCit-ROP6g-DN	ROP6-Promoter	mCitrine vo STOP	mutated (T20N) ROP6 genomic sequence	/	Basta	Kana	pB7m34GW
pROP6:mCITRINE-ROP6gC21S-C158S	ROP6-Promoter	mCitrine no STOP	mutated (C21S-C158S) ROP6 genomic sequence	/	Basta	Kana	pB7m34GW
p35S:mEOS2-ROP6gC21S-C158S	35S-Promoter	mEOS no STOP	mutated (C21S-C158S) ROP6 genomic sequence	/	Basta	Kana	pB7m34GW
p35S:GFP-RBOHD	35S-Promoter	GFP with linker	RBOHD / CDS	/	Basta	Spect	pB7WGF2
p35S:GFP-RBOHF	35S-Promoter	GFP with linker	RBOHF / CDS	/	Basta	Spect	pB7WGF2
p35S:GFP-ROP6	35S-Promoter	GFP with linker	ROP6 / CDS	/	Basta	Spect	pB7WGF2
p35S:RFP-ROP6	35S-Promoter	RFP with linker	ROP6 / CDS	/	Basta	Spect	pB7WGR2
p35S:RFP-ROP6-CA	35S-Promoter	RFP with linker	ROP6-CA (G15V)/ CDS	/	Basta	Spect	pB7WGR2
iROP	35S-Promoter	CRIB of PAK1	mcherry-mvenus	ROP6 / CDS	BASTA	Spect	pB7m34GW

Table S2. List of used expression vectors. Related to Star MethodS

	Name	Sequence
Cloning of PCR fragments	ROP6-B2R	ggggacagctttcttgtacaaagtggctatgagtgcttcaaggtttatcaagtg
	ROP6-B3w3'UTR	ggggacaactttgtataataaagttgccttaagacaattggtgtgaatctagg
	F-RBOHD	cttgcggccgcccccttcaaaatgagacgagg
	R-RBOHD	gcaaggcgcgcccacccttctagaagttctctttgtgg
	F-RBOHF	cttgcggccgcccccttcaaaccgttctcaaagaac
	R-RBOHF	gtcggcgcgcccaccctttagaaatgctccttgtg
	R-ROP6 (CDS)	agcggccgccagtgcttcaaggtttatc
	F-ROP6 (CDS)	tggcgcgccctcagagtatagaacaacc
	ROP6prom-Rev	ttttttgtacaaacttgcctttctctccttcttcaaacttc
	ROP6prom-Fw	gtatagaaaagttgctaacaagctttcagaaaagaggatg

Mutagenesis	ROP6-CA-(G15V)_F	gtcggcgacgttgctgttggaaagacttgtc
	ROP6-CA-5G15V)_R	tccaacagcaacgtcgccgacagtgacacacttgataaacc
	ROP6-DN(T20N)-F	ggtgctgttggaaagaattgtcttctcatctcctacactagc
	ROP6-DN(T20N)-R	atgagaagacaattctttccaacagcaccgtcgccgacagtg
	Mut-C152S_R	gagtttttgcactggattcgatataagcaggcgccccaatcagcttctttagttc
	Mut-C152S_F	atcgaatccagtgcaaaaactcaacaggtattaacctgagagtcaatatctttatc
	Mut-C21S-WT_F	ggaaagacttctcttctcatctcctacactagcaacactttccccacggttagc
	Mut-C21S-WT_R	agatgagaagagaagtctttccaacagcaccgtcgccgacagtgacacacttg

Table S3. List of used oligonucleotides related to Star Methods